Politecnico di Torino

Master's Degree in Environmental and Land Engineering

Climate change

Master's Degree Thesis

On the thermal regime of water in a periglacial lake: the case of the Rutor marginal lake

SUPERVISORS:
Prof.ssa Stefania Tamea
Prof. Jost von Hardenberg

CANDIDATE:
Aida Galfione

Academic Year 2021-2022

October 2022

Contents

Abstract

The Rutor glacier is one of the most important glaciers in the north-west of Italy (Aosta Valley). Due to both climate change related phenomena and to natural cycles it is melting quite fast. Water coming from the melting of the main glacier tongue is converging through a seasonal stream to a lake, located in the periglacial area . The temperature and the water level of this seasonal lake has been measured during the summer period (20th July to mid-September 2021) with a probe. The objective of the work is to create a model that can estimate the temperature of the lake on the basis of the air temperature, the incoming radiation, the wind speed and the relative humidity, measured in the different meteorological stations located close to the lake area. A preliminary analysis on how air and water temperature series are correlated results in a delay of the response of water temperature to air temperature variation. The shift between the two series is higher in the morning and the afternoon, when the most air temperature variation occurs. The model is based on an energy balance equation: the variation in time of the water temperature depends on the thermal flux between the lake water and the air temperature at the lake surface. In the total heat flux, shortwave radiation and longwave radiation heat fluxes are considered, as well as sensible and latent heat fluxes. The lake bed and the banks are assumed to be adiabatic. The obtained equation allows for the evaluation of the temperature variation of the lake water at the hourly time scale, due to the total thermal flux. The equation is solved by numerical integration, resulting in a time series of water temperatures of the lake, starting from a known initial condition. Results variability is investigated considering the contribution of single terms of the energy balance and weighting all the parameters with respect to the real series. The contribution of longwave and shortwave net heat fluxes are contributing more to the total heat flux with respect to sensible and latent heat fluxes. Some temperature fluctuations, wider in the estimated series than in the measured one, are anyway due to the less contributing terms and to neglected fluxes. Even though the resulting series is not perfectly reproducing the measured one, a realistic dynamics and a similar range of values is found. That means that the energy balance approach can be a good one to estimate the water temperature of a water body at this altitude, keeping in mind that further corrections are needed.

1. Rutor glacier

Rutor glacier is located in Aosta Valley, north-west Italy, near the Italy-France border. Rutor glacier is located in La Thuile valley, it is surrounded by mountains of height in the range of 3000-3500 m asl. Its name comes from the highest mountain that is part of the chain surrounding the glacier, Testa del Rutor (1346 m asl). From this glacier river Dora di Verney is originated, which then flows into Dora Baltea. The glacier has a north-north west exposition, and it develops between 2450 and 3440 m asl.

Figure 1.1: *Rutor glacier (source ARPA Vda).*

Rutor glacier is one of the largest glacier in the region, at the bottom of it there are many small lakes. The biggest and most famous lake is Lago dei Seracchi, a marginal lake, located in the valley just at the bottom of the glacier (Figure 1.2). After the maximum holocenic expansion, around 1820, Rutor glacier started to decrease in size, and a relevant morenic structure has been created in the area below the glacier [29]. Rutor glacier, as the other glaciers in the Alpine region, is reducing its size, mainly due to climate change. Climate change in this case concerns a series of phenomena that combined cause the loss of ice thickness and thus the loss in the amount of water available in the glacier as natural water reservoir. Val d'Aosta region is producing yearly a mass balance of this glacier, from 2005. In Figure 1.3 it is represented the temporal series of the glacier mass balance from 2005 to 2019. In the recent years the situation is becoming more dramatic and, as it can be observed

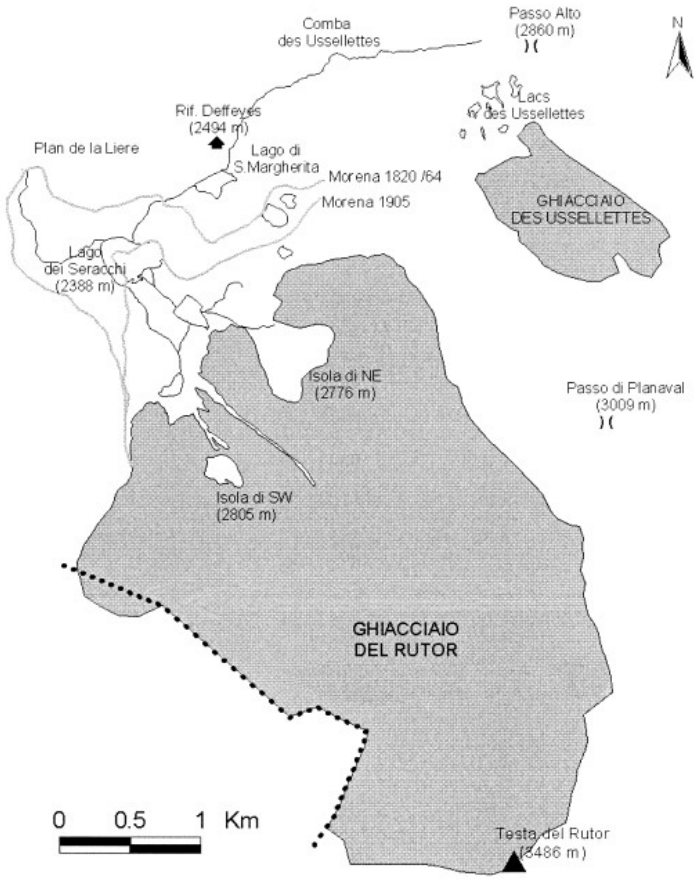

Figure 1.2: *Rutor glacier and its valley [29].*

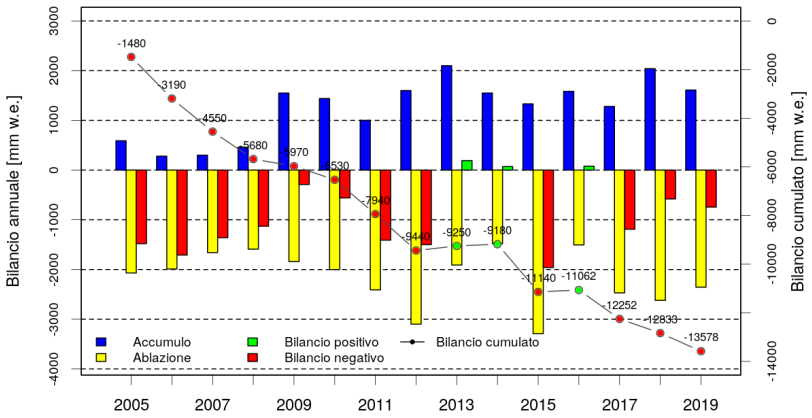

Figure 1.3: *Rutor mass balance 2005-2019 [1].*

from Figure 1.3, the mass balance has almost always been negative. In 2013, 2014 and 2016 it was slightly positive but not in such a way to be very relevant to balance the cumulative mass balance. Negative mass balance have been caused by high summer temperatures that

enhanced ice melting, reduced winter precipitation not allowing for consistent accumulation, or both the processes combined. To be noticed the 2018 and 2019 situation: although the blue bar (accumulation) is high, the annual mass balance is negative, due to the very high summer temperatures. A similar trend is found also for other glaciers in the same area [1]. Thus, the effect of climate change is evident: monitoring, mitigation and adaptation strategies and actions are needed.
As from the last ARPA VdA report (June 21st, 2022), in which the results about the assessment of snow accumulation at the Rutor glacier and at the Timorion glacier, it is stated that the snow accumulation at the Rutor glacier is higher with respect to the more internal part of the region (Figure 1.4). This trend is probably due to its location close to France, that allowed for an enhanced influence of Atlantic perturbations, increased by orographic effect at the french border. The snow accumulation is 1077 mm of snow water equivalent, a value

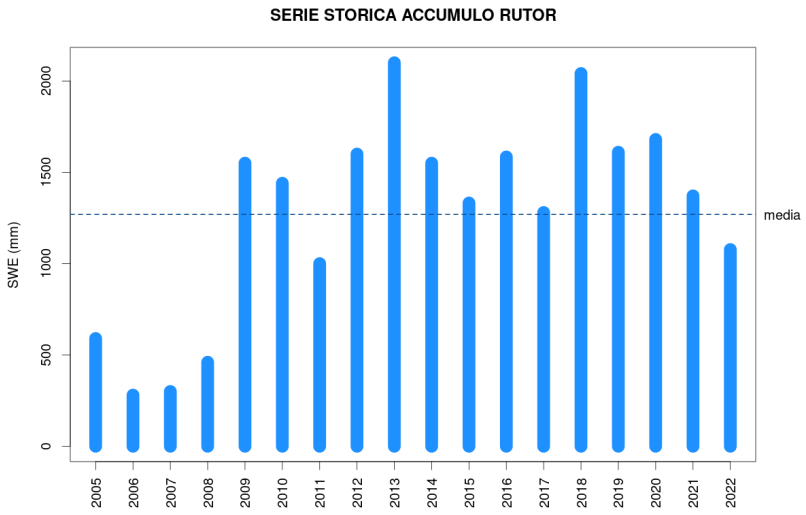

Figure 1.4: *Historical series of snow accumulation 2005-2022 [2].*

that ranks the 2021-2022 winter season as the sixth position ever for mass scarcity, with values slightly lower than the mean of last years [2].

The history of Rutor glacier is populated by a series of important outbursts and glacier floods, the last one occurred in 1933 [43] [3]. All the recorded glacier floods happened from outbursts of proglacial lakes, due to front fluctuations.

2. Proglacial lakes - Glacial environment

Proglacial lakes are increasing in areal extent and in number globally. This number will continue increasing as glacier overdeepenings become ice-free and fill with meltwater. Some of these lakes have been found to be linked to ice sheet destabilization and are thought to have been a control on ice stream onset and dynamics, although these effects are still not tested into numerical models [14].

Ice-marginal lakes interact with glaciers through a series of thermomechanical processes (Figure 2.1). These processes are combined with climatic effects, and they can interact with them via feedback mechanism. Temporary destabilisation of an ice-margin can cause calving: drawdown of ice is caused and ice surfaces are steepened. A hydraulic connection is established between a subglacial drainage system and lake water that reduces bed friction and longitudinal stresses. Glacier flow speeds are expected to increase, with a bed friction reduction. The result is a glacier thinning and a positive feedback is introduced: effective pressure decreases, basal ice motion is enhanced and flow velocity is further enhanced [14].

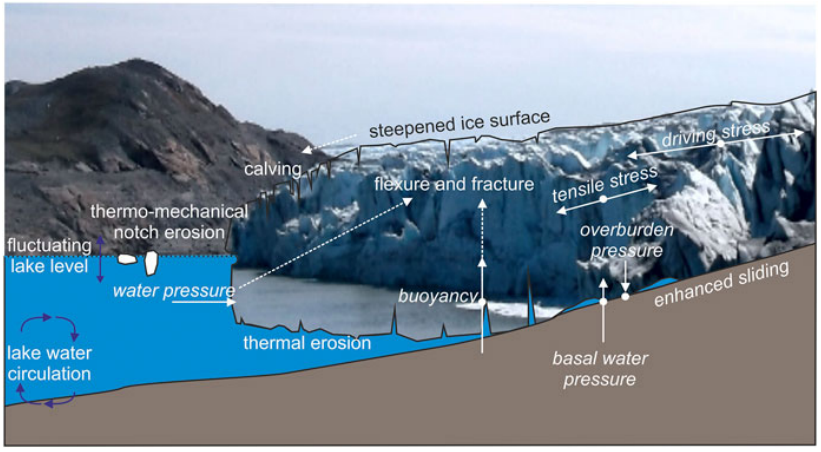

Figure 2.1: *Schematic of most important components of ice-marginal lake and glacier interactions [14].*

Ice-marginal lakes alter significantly the longitudinal stresses and the flow regime of a glacier and that effect can propagate up-ice from the terminus. Remote sensing and field data

analysis have both showed that the presence of ice-marginal lakes alters glacial thickness, being considered a dynamic thinning mechanism. The positive feedback between glacier mass loss and meltwater feeding, makes the water level fluctuating, often by tens of meters. Dynamic water level is tough to consider and technically and computationally difficult to achieve [14].

Ice-marginal lake water temperature dramatically affects subacqueous melt rate, but unfortunately it is rarely quantified. On a small (meters) scale, thermo-mechanical notch development will be affected by lake water temperature. On a meso-scale, lake temperature affects subglacial hydrology. On a macro scale, lake water temperature will affect the shape of the floating underside of a glacier and potentially also affect the shape of the entire terminal tongue.
Subglacial hydrology is affected by lake water temperature at all scales. Lakes can affect local surface energy balance via an albedo effect, as well as a thermal heat capacity effect. lake water temperature and air albedo influence local air movements, and lake water circulation currents can be driven by valley winds. As a result, the local surface energy balance is modified and the wind has the potential of enhancing thermal undercutting and calving: the dimension of these phenomena is still unquantified, although it is reasonably proportional to lake size. In addition, very large lakes can act as moisture source, increasing precipitation locally on the ice sheet [14]. Thermal regime of proglacial lakes can be a good indicator to assess the dynamics going on at the lower bound of a glacier, when associated to other products as mass balance analysis, remote sensing and geomatics products, hydrological analysis.

Aosta Valley is the region with the largest glacierized area of Italy. Like other high mountain regions, it has shown a significant glacier retreat starting from the end of the 'Little Ice Age' that is expected to continue in the future. As a direct consequence of glacier shrinkage, glacier-bed overdeepenings become exposed, offering suitable geomorphological conditions for glacier lakes formation. In such a densely populated and developed region, risks connected to lakes may arise. One of the potential risks is due to outbursts and consequent floods, the element at risk are the villeges located at the bottom of the valley and the mountain infrastructures (ski infrastructures, alpinism equipment) in the area. Glacier lakes formation also brings some opportunities: the economic exploitation of accumulated water for hydropower production, tourism and water supply and the environmental relevance for high mountain biodiversity and geodiversity [43].

3. Thermal regime - physical phenomena

Water temperature has both ecological and economic linkages, connected to fish life, reproduction and species protection. It is related to many environmental and physical mechanisms, such as air temperature, elevation, weather, turbulence, climate. Air temperature is one of the main drivers of water thermal regime in mountain streams. Elements that affect more the thermal regime of rivers are [20]:

1. **Air temperature**. Atmospheric conditions are the main responsible of heat exchange between air and water, occurring at the water surface, including phase changes. Models predicting water temperature of water bodies very often use the relation between air temperature and water temperature, via heat fluxes estimation. However, the relation between air temperature and stream water can be problematic to be estimated, especially in mountainous, high elevation areas. In general, water warms up at a slower rate with respect to air, because it has an higher heat capacity; thus, there can be an over-prediction of stream water temperature, mainly due to stream-scale elements, such as vegetation and groundwater/sediments contributions, which buffer high elevation water bodies from rising air temperatures [26]. Different studies model the air-water temperature relation with a simple linear regression, but enough attention has to be spent in analysing the temporal and geographical resolution of each study. Departures from linearity have been noticed mainly at low and high temperatures, when the near-exponential increase of near-water-surface vapour pressure enhances evaporation and evaporative heat loss which imposes an upper bound change on stream and river temperatures [44]. Radiative flux is for sure the most impacting environmental driver for water temperature changes, but many other factors have to be accounted for, and their influence on stream temperature has to be quantified. However, air temperature trend is generally followed by water trend; when reducing the timescale, the differences between the two trends enlarges [25].

2. **Low flow**. It has been observed that air temperature influences more markedly water temperature when the flow is low. One of the causes is that, when flow is low,

the depth of the water body is reduced too. Higher discharge leads to higher inertia to air temperature [20]. Low flow and low thermal inertia of shallow water bodies can increase the evapotranspiration phenomena, thus increasing in turn water temperature [37]. Stream discharge is mainly due to the river hydraulics, and affects mostly the heating capacity of the water body, and the cooling through mixing water from different sources, including streambed heat exchanges [13].

3. **Elevation and stream slope**. Trials have been performed to classify rivers depending on latitude and longitude, but no significant results have been found. The complexity of thermal phenomena affecting river temperature variability was highlighted. Topography is an important factor because it influences atmospheric conditions and so air temperature [13]. Higher elevation meteorological stations usually record lower air temperatures. Therefore, water temperature is generally lower when elevation is higher [20].

4. **Land cover**. It has been demonstrated many times already that timber harvesting affects significantly river water temperature, especially in small streams, due to the small thermal capacity of the low water volume. In addition, it has been demonstrated that the daily variation is not only function of the stream dimension but it also depends on seasonal fluctuations. Peak flows and snow melt can play an important role in the overall temperature variability [13].

5. **Hyporheic zone**. The hyporheic zone also controls a river's thermal dynamics. This zone is the locus of complex exchanges (water, nutrients, organic matter, etc.) between groundwater and surface water. Hyporheic exchange influences spatial and temporal stream temperature variability. Especially during the summer months, cooler groundwater mixed with warmer mainstream water dampens water temperature rise and decreases maximum water temperature. Numerous studies demonstrate that the hyporheic zone plays an important role in mitigating water temperature rise [20].

6. **Riverbed and groundwater heat exchanges**. Rivers with shallow groundwater signatures show higher proportions of warming with respect to other streams with deeper water signatures, probably due to the buffering of this and other factors [25]. By Caissie (2006), it is stated that river water temperature is close to groundwater temperature near the source, then it increases down stream, in general. The increase in temperature downstream is not linear and it is larger for small rivers with respect to high discharge ones. It is notable that for small stream the temperature variability is of the order of $0.6^{\circ}\text{C km}^{-1}$, while significantly lower for larger rivers ($0.09^{\circ}\text{C km}^{-1}$) [13].

4. Thermal regime under climate change

Climate change has been identified to be one of the main driver of river thermal regime recently. Climate change is able to modify significantly the distribution of aquatic species, as water temperature in some streams already reached the lethal limit for selected organisms [13]. Under climate change temporal series of air and water temperatures have been observed to increase their autocorrelation. The same behaviour has been observed on spatial fields. Increased spatial autocorrelation and temporal variance result in more direct consequences for ecological systems. This both spatial and temporal persistence of harsh conditions (heat waves, droughts,..) can increase biological extinction risk and environmental damage risks [16].

Making prediction on water temperatures and water bodies thermal regime is fundamental in a framework in which climate change will play a major role in the future [30]. The temperature estimation is strongly linked to the ecology of the water stream, to the water quality and to the river species population. Using a lake model forced by 21st century climate projections, Maberly et al. (2020) [30] found that 12%, 27% and 66% of lakes will change to a lower latitude thermal region by 2080–2099 for low, medium and high greenhouse gas concentration trajectories (Representative Concentration Pathways 2.6, 6.0 and 8.5) respectively. Thermal regions have been defined through a lake surface temperature analysis, using satellite data, taking into account ice cover. The seasonal trend of the lake has been estrapolated and classified; elevation has played an important role in the classification [30]. The lakes in the dataset were typically large lakes, so that satellite data could be used. The applicability of the resulting classification to small lakes makes some issues arising. Most part of lakes globally are smaller with respect the ones used for the classification. It is known that lake area influences various components of the water heat budget, among others the effects of atmospheric stability, wind speed, turbulent surface fluxes and the diel cycle of surface temperature. To demonstrate the applicability of the model to smaller lakes, local in situ data on seasonal surface temperature from several small lakes have been used. The study concluded that the classification of thermal regions can be used for small lakes too [30].

Climate change will affect hydrologic and thermal regime of rivers, with consequences both for the freshwater ecosystems and the human water usage [35]. The sensitivity in thermal regime changes will be exacerbated by projected decrease in low flow, thus resulting in a lower thermal capacity. Strongly seasonal rivers will experience further increase in water temperature during low flow periods, mainly due to change in the atmospheric energy input [42]. Most studies reveal a future increase in water temperature due to consistent increase in air temperature. Increases are largely attributed to warming air temperatures, but also to lower streamflow volumes which reduce thermal capacity. Some studies suggest that up to 26% of the increases in high water temperature can be indirectly attributed to low flow changes [42] [37]. Anticipated warming air temperatures, changing precipitation patterns, and rising sea levels are expected to alter watershed hydrologic and biogeochemical processes, with direct and cascading effects on water quality. Warming air temperatures have been linked to intensification of the hydrological cycle (e.g., atmospheric water content and changing precipitation patterns) and altered biogeochemical processes — key drivers of water quality [37]. The risk of water quality degradation can be greater during extreme high and low flow events. The main effect of climate change in the Alps is expected to be the increasing in flow variability, including a greater proportion of annual precipitation occurring in heavy events, and longer dry periods between events. In many watersheds, longer summer dry periods, increases in air temperature and and in evapotranspiration are expected to worse low flow conditions, concentrating pollutant inputs [37]. Uncertainty has to be considered as well, since the location, the timing and the human influence can drive in a different way the trend of changes. Concerning the Alps area, it has been studied that the largest warming and cooling anomalies happened at human impacted sites and during summer months [25].

Climate change impacts have been analysed as a factor that impacts on water thermal regime: it remains a research issue due to the lack of data, both on the spatial and the temporal scale. Projected changes in aquatic habitat due to climate change are mainly related to air temperature, although changes in groundwater temperature are also expected. Climate change will not only modify the river thermal regime but other river processes are also expected to be significantly modified, which will impact on habitat creation and existence and on fisheries resources [13].

5. Water temperature models

As reported by Caissie (2006) [13], water temperature models can be classified into three main groups: deterministic, regression and stochastic models. Deterministic models predict water temperature from an energy budget approach, while regression and stochastic models instead employ mainly air temperature to predict river water temperature.

It has been observed that small streams warm up faster down stream, and an equilibrium is reached as soon as average water temperature doesn't differ much any more from average air temperature.

5.1 Regression models

Among regression models, at weekly/monthly time scale linear regression models (Eq. 5.1) have been used in literature, with a certain level of reliability, since at this time scale the water temperature is not generally autocorrelated within the time series.

$$T_w = aT_a + b \tag{5.1}$$

where:
T_w Water temperature [K]
T_a Air temperature [K]
a, b Linear regression coefficients [-], [K]
The point is, though, that when using simple regression models different relationships between air and water temperature can yield at different time scales. Studies have shown that there is a general increase in slope and intercept in the regression line of water on air temperature, as longer time scales are considered. The parameters of the regression line are also function of the stream type (large impact of the streambed heat flux: groundwater dominated streams tend to have less steep slopes with higher intercept, while non-groundwater dominated streams have steeper slopes and intercept closer to the origin) [13].

Multiple regression models instead of simple regression ones have been used as well to predict river water temperature. Logistic regression models have been found in the literature as well, used for the same purpose. In these more complex models, also discharge, time lag data are used, in addition to air temperature. More complex regression models with respect to linear regression have been used after the assumption that the relationship between air and water temperature is not linear: for example it can be affected by different physical phenomena such as evaporative cooling [13].

5.2 Stochastic models

More used if the time scale is larger, with for example daily time steps. Stochastic models are simpler with respect to deterministic models, because they just require data about air temperature as input parameter. Usually in stochastic models the long-term component (annual cycle) and the short-term component are separated. The long-term component is linked to seasonal cycles, and it is well represented with a Fourier series. Concerning the short-term component, it can be modeled with Markov processes and/or the Box and Jenkins method [8], considering both the autocorrelation within the water temperature time series and the relation to air temperature series. Stochastic models can be considered a valuable modelling technique for river water temperature at daily time step, especially when the only available data are air temperature. In the literature stochastic models with good fitting (less than 2°C root mean square error) have been found [13].

5.3 Deterministic models

Deterministic models, as stochastic models, are more often used when the time step is at the daily scale. Many data are needed: basically deterministic models use all the available meteorological data to calculate the energy components. The objective of deterministic models is to fit the total energy flux, previously calculated, to observed changes in water temperature. First models in time used mainly the air/water interface heat flux, while more recent models use streambed heat flux too. it has been noticed to be relevant to consider both heat fluxes, especially when modelling data at hourly time scale [13].

Deterministic models, differently from stochastic and regression models, can predict temperatures with a spatial dimension: they can both carried out at specific sites (0D) or with some spatial dimensions. However the most common deterministic models are computed in a 1D configuration, with the direction of the river set as the principal axis (water of the river is assumed to be well mixed). Larger variability is expected in presence of tributaries,

confluences with other rivers: in this case a site specific analysis with the three spatial components is needed to better assess the mixing process and the eventual solute transport [13].

5.4 Main modelling issues

When modelling the stream temperature, starting from the air temperature, a non linear relation can be observed in general. The non linearity is enhanced at high and low temperatures. At high temperatures, evaporative cooling slows the warming of the stream water, whereas at low air temperatures, air temperatures can dip well below the water temperature freezing limit. If the analyses is limited to the summer, as many models do, the non linearity is limited, since the problem of the heterogeneity of variance among temperatures in the around zero interval is avoided [28].
Due to thermal inertia, stream temperatures don't respond immediately to air temperature. Including time lags in air temperature can improve the performance of the model, especially at short time scales [28]. The effect of the lags increases with the depth of the stream and with the stream flow.
The amount of data of stream temperature available worldwide is increasing, but still many issues on their completeness are present. Missing data in many study regions, both for some hours or for an entire year may be missing, can affect the model result, depending on how the model is constructed. A linear model is less sensitive in general to missing data, while non linear models can be dramatically affected as missing data can fail to shape the non linear curve.
Spatial and temporal autocorrelation can cause estimation problems. When constructing a model from a temporal or spatial series, the best condition would be to have all independent data, but unfortunately, usually, is not so. For example, concerning stream temperatures, spatial correlation can occur between temperatures measured upstream and down stream; concerning temporal correlation, in the air temperature series, there can be correlation between one day and the day after [28].
Solar radiation is one of the key variables in such models. When setting an energy balance in a point or over a certain surface, solar radiation at that point or surface needs to be evaluated. Solar radiation at the surface can be splitted into two main components, shortwave and longwave solar radiation. To evaluate the direct contribution of shortwave radiation, the amount of solar radiation recorded by the instruments is used. To evaluate the incoming longwave radiation the relation is more complex. In an ideal blackbody infrared radiation would follow Stefan-Boltzmann law, but in the real case many factors as cloud cover, atmospheric scattering, light can influence the model.

Finally, air temperatures are not the only important factors influencing stream water temperature. It is important to include in models also environmental and landscape drivers. Landscape drivers that can be included are: topography, riparian cover, stream depth. Environmental drivers often include: stream flow, snow melt, groundwater contribution, humidity. If the study site is small and the data can be considered compliant with the actual situation, topography in general can be avoided to be inserted within the drivers of the model [28].

6. Energy balance at the surface - heat exchange

Concerning air temperature, heat exchange between air and water occurs at the water surface. The exchange occurs through solar radiation, but also through sensible and latent heat. When comparing energy components, net short wave radiation is the dominant one, followed by long-wave radiation, and evaporative heat flux. Sensible heat flux is the smallest component of the total energy flux, although it is not negligible. In general, it has been found that the majority of the heat exchanged came from the air/water surface flux (82% of the total heat flux [19]).
Concerning small streams and water bodies, mostly due to the massive presence of sheltering and shading, there are still relevant uncertainties in quantifying the entity of each thermal flux component. While for large streams it is fair to assume that the heat flux that dominates the heat exchange is the one occurring at the water/air interface, due to the incoming solar radiation and to the wind, for smaller streams instead, as the presence of vegetation becomes more important, shading effect reduces significantly solar radiation and wind speed. As a consequence, streambed heat flux gains importance with respect to the water-air heat flux [13]. The total heat flux (in W/m^2), comprehensive of all components that can produce an exchange of heat between water and another element, can be expressed as [36]:

$$H_{total} = H_{sw} + H_{lw} + H_s + H_l + H_b + H_a \tag{6.1}$$

where:
H_{sw} Net shortwave radiation [W/m^2]
H_{lw} Net longwave radiation [W/m^2]
H_s Sensible heat flux [W/m^2]
H_l Latent heat flux [W/m^2]
H_b Fluxes to/from the river bed [W/m^2]
H_a Heat fluxes due to groundwater and tributary inflows [W/m^2]

Every component of Eq. 8.9 is worth a more detailed discussion, that will be held in the following. The complete scheme of the physical phenomena occurring in the analysed situation is summarised in Figure 6.1.

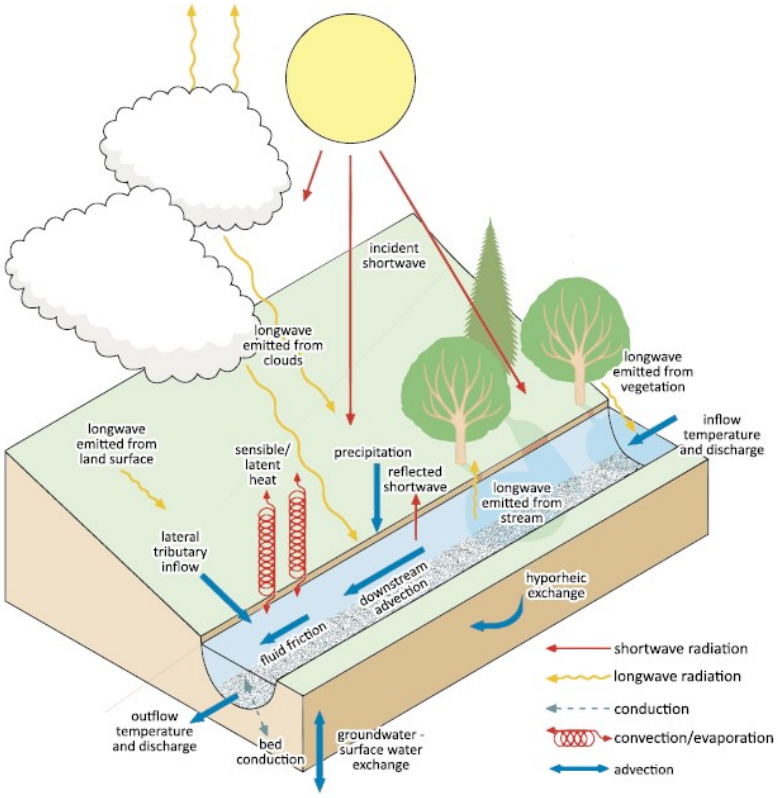

Figure 6.1: *Energy and hydrological exchanges determining stream temperature [17].*

6.1 Shortwave radiative flux

As already mentioned above, the shortwave radiative flux is the main component of the total energy budget. Shortwave refers to the light in the range of wavelength between 0.4 µm and 4.0 µm. In general, concerning available data, solar radiation measurements are much more scarce with respect to air temperature, precipitation and air humidity [36]. Since solar radiation can vary with latitude, season and time of the day, it can be estimated via full radiative models, and it is usually done in atmospheric and meteorological models. The amount of shortwave radiation reaching the target location varies cloud cover and surface albedo, making it more complex to reasonably estimate it. In addition, the fraction of shortwave radiation that penetrates the water body depends on a number of factors, such as water color and turbidity [17].

Short wave radiative flux accounts for the main component of the energy balance during

summer months in glacial environment. Thus there can be a big error in the evaluation of this component in the energy balance, leading to the need of a punctual evaluation. Shortwave radiation flux is the controlling one for the glacier melting phenomenon: the summer period matches with the ablation period for the glacier, albedo is low and the melting process is ongoing. Remote sensing applications and Digital Elevation Model (DEM) have been used by Olson et al. (2019) to model incoming shortwave irradiance, considering that slope and aspect (combined) and topographic shading have the greatest impact on daily shortwave irradiance. This study has been applied to a number of glaciers in Asia, in the Everest region. It has been reported that the coarser the resolution of the model, the more acceptable the bias on the shortwave incoming radiation. When the resolution of the model gets higher, the bias increases considerably [34].

Incident shortwave radiation can be divided into three components:

- Direct beam irradiance
- Scattered diffuse irradiance
- Reflected irradiance

Different topography can either enhance or reduce the amount of incident solar radiation. Slope and aspect, generally combined, can affect the direct beam irradiance: by changing the solar zenith angle relative to a flat plane, a north facing slope will receive less radiation with respect to a flat plane, whereas a south facing slope will receive more radiation.

In mountainous areas, slope and aspect are generally assumed to be the most relevant factor in regulating the absorbed solar radiation at the surface. In steep alpine terrain, topographic shading can't be neglected. Due to the high spatial and temporal variability of the angle and of the topographic components throughout the day, the correct assessment of the relative importance of each contribution can be challenging [33].

To get the net shortwave radiation contributing to the whole energy balance, the fraction of reflected radiation with respect to the incident amount is needed. For the calculation of this term, the albedo feedback is exploited.

6.2 Longwave radiative flux

Longwave radiation is defined at waves with wavelength larger than 4.0 µm. Its flux can vary affected by temperature and humidity at low latitudes. The law that describes such

flux is the Stefan-Boltzmann law, in which it is stated that the energy radiated from a black body surface is proportional to its temperature to the fourth power. In the case of a water body, incoming longwave radiation component is estimated from air temperature ($\propto T_a^4$). Most largely used in models for computing the longwave radiative flux are semi-empirical equations, in which air temperature, and sometimes also sky emissivity and cloud cover are considered [36]. Air temperature data are usually available data from meteorological stations, nearby the target. A more complex and challenging evaluation concerns sky emissivity. Berger and Bathiebo (2003) [5] set up a simplified model for the directional sky emissivity calculation, relying on the Bliss method. Sky radiation consist in a heat loss, equivalent of that a black body, but cooler of about 30°C than a black body at ambient air temperature. The contribution of each atmospheric constituent to the absorption of the infrared radiation can be summarised as:

- The absorption spectrum of the water vapor is composed by two parts: a discontinuous absorption (lines) in the range $3-50\,\mu m$ and a continuous absorption, overlapping of the wings of the outside absorption lines
- A peak at $9.6\,\mu m$ due to ozone
- A wide band in the range $13-17\,\mu m$ due to CO_2 and other uniformly mixed gases
- A weak band at $7.6\,\mu m$ due to CH_4

As first approximation, the clear sky condition is evaluated. A certain number of empirical equation, starting from meteorological quantities that have been measured, such as air temperature and humidity are reported [41]. Ouellet at al. (2012) reported in their review the most common formulation for calculating the total clear-sky atmospheric emissivity (Eq. 6.2-6.6).

$$\varepsilon_m = 1 - a_1 \exp\left[b_1 (273 - T_a)^2\right] \tag{6.2}$$

$$\varepsilon_m = a_2 \left(\frac{e}{T_a}\right)_2^b \tag{6.3}$$

$$\varepsilon_m = a_3 + b_3 e^{\frac{1}{2}} \tag{6.4}$$

$$\varepsilon_m = a_4 1 - \exp\left[-e^{\left(\frac{T_a}{b_4}\right)}\right] \tag{6.5}$$

$$\varepsilon_m = a_5 + b_5 \exp\left[\frac{c_5}{T_a}\sigma (T_a)^4\right] \tag{6.6}$$

where:
T_a Air temperature [K]

σ Stefan-Boltzmann constant [W/m^{2}K^4]
The constants appearing in the above equations have been defined from the authors as [41]:
$a_1 = 0.261$, $b_1 = -7.77 \times 10^{-4}$
$a_2 = 1.24$, $b_2 = \frac{1}{7}$
$a_3 = 0.605$, $b_3 = 0.048$
$a_4 = 1.08$, $b_4 = 2016$
$a_5 = 0.70$, $b_5 = 5.95 \times 10^{-5}$, $c_5 = 1500$
The above equations can be solved with the available data of temperature at the target, getting different estimations of teh clear sky emissivity. When computing the sky emissivity using bulk equations 6.2 to 6.6, the values obtained are between 0.6 and 0.7. These values are perfectly compliant with literature values.

These equations assume clear sky and standard conditions for the atmosphere. The simplification consists essentially of assuming an isotropic source function in a stratified atmosphere for which absorption coefficient and temperature are functions of elevation only. In general it is not simple to retrieve radiation data, thus an empirical equation deduced from the basic assumption of Stefan-Boltzmann law validity, so based only on ground temperature, can be a good solution to the problem [11].

During clear sky days the longwave downward radiative flux can be simply estimated by applying teh stefan-Boltzmann law, and using the previously estimated and discussed sky emissivity values. But it has to be considered that not all the days are without clouds. Clouds are a very important factor for the Earth's climate. Clouds are a key factor in regulating the Earth's radiative balance: both the planetary albedo and the surface fluxes depend to a certain extent on the cloud cover. clouds absorb longwave radiation emitted from the Earth and emit them back downward. This trapping mechanism tends to warm up the Earth surface. Therefore, the cloud cover must be taken into account when trying to set an equation for Earth's surface energy balance. The cloud forcing is a tough variable to be measured, and comparison between satellite measures and GCM estimations highlighted often large differences [31].
Once calculated the total sky emissivity, longwave downward radiative flux has to be estimated. The reported semi-empirical models from Ouellet et al. (2012) are all based on the Stefan-Boltzmann law, what differs is how sky emissivity, temperature and eventually cloud cover are combined together.

$$H_{lwd} = \varepsilon_m C^b \sigma T_a^4 \tag{6.7}$$

where:
T_a Air temperature [K]
ε_m Sky emissivity [-]

σ Stefan-Boltzmann constant [W/m^{2}K^4]
C Cloud cover (0-1) [-]
b Empirical coefficient [-]

Eq. 6.7 (from Brutsaert, 1993) is based on Stefan-Boltzmann law. Sky emissivity has been evaluated as explained above from the ground temperature, including some empirical coefficients. The cloud cover appears in the equation as it is one of the main drivers when estimating the net longwave heat flux. If the cloud cover term is not considered, then the formula could be reasonably applied only during clear sky days. Since clouds play a major role in infrared radiation management in the atmosphere, it wouldn't be consistent to neglect the C term. Eq. 6.7 express the downward longwave flux [41].

The reflected part to get the net flux is particularly difficult to be estimated: it depends on many atmospheric parameters such as the air particles content, that are not simple to be parameterised. At the considered latitude, after Fresnel, it is reasonable to consider that the reflected fraction of longwave radiation is about the 3-4% of the incident flux [36]. To be compliant with the physical phenomena occurring at the lake surface, the upward longwave flux can be estimated as the infrared radiation emitted from the lake at any time, given its water temperature. Water emissivity can be considered to be $\varepsilon_w = 0.99$ [23]. Following the Stefan-Boltzmann law, the emitted longwave radiation from the lake can be estimated as

$$H_{lwu} = \varepsilon_w \sigma T_w^4 \tag{6.8}$$

where:
T_w Water temperature [K]
ε_w Water emissivity [-]
σ Stefan-Boltzmann constant [W/m^{2}K^4]
Once estimated both the upward and the downward contribution of longwave radiation, the net longwave radiative flux (in W/m^2) is estimated as

$$H_{lw} = H_{lwd} - H_{lwu} \tag{6.9}$$

Water surface has an high emissivity in the thermal infrared band, that can explain why such an high value for ε_w has been used. Of course the emissivity depends on water temperature and on turbidity. The surrounding environment characteristics can't be neglected, since they are affecting water emissivity as well [6].

6.3 Latent heat flux

Latent heat flux is the heat exchanged due to water evaporation. The evaporation flux is a function of the saturated air and the air pressure coefficient, modulated by a wind velocity function. The difficulty in parametrizing this significant heat component for the energy balance, led to the numerous formulations present in the literature. The base equation for calculating the latent heat flux is

$$H_e = \rho_a L_e \overline{E} \tag{6.10}$$

where:
ρ_W Air density [Kg/m^3]
L_e Latent heat of vaporisation [kJ/Kg]
$\overline{E}$ Rate of evaporation [m^3/s]
What differs among the formulations in the literature is how $\overline{E}$ is calculated. Most of the models are based on Dalton's law of partial pressures, thus computing the evaporation rate using the actual vapor pressure and the saturation vapor pressure [17]. Ouellet et al. (2012) reported some bulk equations for H_e calculation most widely found in the literature (Eq. 6.11-6.16).

$$H_e = 1.141 \left(\frac{\alpha}{\alpha - 1}\right)\left(\frac{\gamma}{S+\gamma}\right)\left(\frac{(2.9+2.1V)(E_s - E_a)}{L}\right) \tag{6.11}$$

$$H_e = \frac{S}{0.85S + 0.63\gamma}\frac{Q_n - Q_x}{L} \tag{6.12}$$

$$H_e = N_m V (E_s - E_a) \tag{6.13}$$

$$H_e = \left(\frac{S}{S+\gamma}\frac{Q_n - Q_x}{L}\right) + \left(\frac{\gamma}{S+\gamma}(15.36(0.5+0.01V)(E_s - E_a))\right) \tag{6.14}$$

$$H_e = \left((2\alpha - 1)\left(\frac{S}{S+\gamma}\frac{Q_n - Q_x}{L}\right)\right) - \left(\frac{\gamma}{S+\gamma}(0.26(1+0.86V(E_s - E_a)))\right) \tag{6.15}$$

$$H_e = \alpha\frac{S}{S+\gamma}\frac{Q_n - Q_x}{L\rho} \tag{6.16}$$

where:
E_s Water vapor pressure [kPa]
E_a Air vapor pressure [kPa]
α Priestly-Taylor empirically derived constant [-]
S Slope of saturated vapor pressure [Pa/K]
γ Psychrometric constant [Pa/K]
V Wind velocity at 2 m [m/s]
Q_n Net radiation [W/m^2]
Q_x Change in heat stored in the water body [W/m^2]

L Latent heat of vaporisation [MJ/Kg]
N_m Mass transfer coefficient [-]
ρ Water density [Kg/m^3]

Eq. 6.11 refers to the model equation for calculating the evaporative flux, set by De Bruin, 1978. By combining the empirical model of Prestley and Taylor (1972) for evaporation of saturated surfaces and the Penman equation (evaporation from an open water surface), evaporation equation for a shallow lake has been obtained. Wind velocity, Prestley-Taylor constant, latent heat of vaporisation and air and water vapor pressure are present in the equation. α can be assumed with a constant value of 1.26. Vapor pressures and wind velocity have to be measured at 2 m [9].
Eq. 6.12 has been set by combining the empirical model of Prestley and Taylor (1972) with the observation data of a lake in the Netherlands, in the summer period. Form the comparison between modeled data and observations, it has been found that α has a pronounced seasonal variability [10].
Eq. 6.13 considers the mass transfer coefficient, the wind speed and the vapor pressures. To properly evaluate N_m coefficient, the authors relied on the logarithmic wind law and a law describing humidity variation with the form of a Pearson function, provided by Calder (1949). Once selected the saturation vapor concentration, α and the lake depth, N_m can be evaluated, according to Eq. 6.13 and thus the evaporative flux is obtained [21].
Eq. 6.14 has been obtained by comparing daily and periodic evaporation from different surfaces, by Penman (1948). What the author did is to consider the energy balance over the water surface and the sink strength to evaluate the total evaporative flux. The first approach is based on the energy components, and evaporation is regarded as one of the ways of degrading incoming radiation; the second approach has an aerodynamic basis in which evaporation is regarded as due to turbulent transport of vapour by a process of eddy diffusion [39].
Eq. 6.15 is derived in the context of evapotranspiration. The concept of aridity, regarded as absence of water for evapotranspiration, is opposite to the potential evapotranspiration. Latent heat and the change in heat stored in the body water as well as air and water vapor pressure are considered in such estimation [12]. Eq. 6.16 is related to the high variability noticed in water evaporation from the lake is strictly linked to the daily variability in water and air temperature. The effects of these changes are emphasized in the highly fluctuating changes in the heat storage of the lake during daylight hours. Much of the energy utilized in warming the lake is later released as evaporation during the night when the lake is cooling. Evaporation from a surface over any time period can be expressed as a function of equilibrium evaporation. α is assumed to be in the range 0-1.26, but it can be considered almost constant at 1.26 ($\alpha = 0$ means that no evaporation occurs). Hence if α is known, variations

in the evaporative flux can be calculated from a knowledge of temperature and available energy [40].

6.4 Sensible heat flux

The magnitude of the sensible heat flux is generally lower with respect to radiative and latent heat fluxes [13]. However, the contribution of sensible heat flux is not negligible, acting as a heat sink during winter period and as a heat source in summer months. Most of the reviewed energy models calculated the sensible heat component in a similar way, starting from the Bowen theory (1926) [7]. This results in little discrepancies among the different models from the literature, meaning that the model selection is generally driven by more significant components of the energy balance [17].

The sensible heat flux is primarily influenced by temperature and pressure differences that are modulated by the wind speed. As cited before, most of the formulation are built after Bowen model (1926), thus contain the Bowen coefficient β. For sake of consistency, the same wind function proposed by Brady (1969) for the latent heat flux has been used, getting the formulation [36]:

$$H_c = 4.28\beta\left(19 + 0.95V^2\right) \tag{6.17}$$

where the Bowen coefficient β (dimensionless) is defined as:

$$\beta = \frac{T_w - T_a}{E_s - E_a}\frac{P_{atm}}{P_0} \tag{6.18}$$

where:
T_w Water temperature [K]
T_a Air temperature [K]
V Wind velocity at 2 m [m/s]
E_s Water vapor pressure [kPa]
E_a Air vapor pressure [kPa]
P_{atm} Atmospheric pressure [kPa]
P_0 Mean tropospheric pressure at sea level [kPa]

The vapor pressures are calculated with the Magnus-Tetens equations [36]:

$$E_s = 610.78\exp\left[\frac{17.26939T_a}{T_a + 273.29}\right] \tag{6.19}$$

$$E_a = \frac{RH}{100} E_s \tag{6.20}$$

where:
T_w Water temperature [C°]
T_a Air temperature [C°]
RH Relative air humidity [%]

6.5 Fluxes to/from the river bed

The heat flux to and from the bed of the lake/river is an important contribution to the overall heat flux. It accounts for around the 15% of the total heat flux. The heat exchange occurs also at the streambed/water interface, although it has received less attention, especially on the modelling side. The main reasons of streambed heat flux is the geothermal heating through conduction and of advective heat transfer through groundwater contribution and hyporheic exchange. Intergravel water temperature have shown that rivers are usually cooled down by groundwater in summer through stream bed heat fluxes, while in winter this heat is released from the river. This heat exchange mechanism is very important in autumn, for the significant thermal gradient resulting from the summer heating accumulated in the ground [13]. The total exchange at the channel bed comprises:

- heat flux due to net bed radiation
- heat flux due to bed conduction
- heat flux due to convective heat transfers with bed
- heat flux due to advective heat transfers with bed
- heat storage within the bed.

The water column, in addition to the heat exchange that occurs at the air-water surface, can exchange heat at the channel bed interface and can gain energy through friction at the bed and banks interfaces [19]. In general all these contribution are not negligible, but given the absence of data referring to the specific site of interest, this contribution has been neglected within the total heat transfer equation.

6.6 Heat fluxes due to groundwater and tributary inflows

Fluxes from groundwater and tributary inflows are for sure not negligible. Given the environment in which the site of interest is located, infiltration of water from the melting

process is expected, as well as different inflow discharge from the runoff water from the glacier melting. Due to the scarcity of data and to the strong seasonality of this contribution, in this specific work such a contribution has been neglected.

7. Data analysis

As first step, the availability of data has been checked. The multiparametric probe installed from the Politecnico equipe recorded some data on a side of the lake. The lake this work is referring to is a marginal lake that forms seasonally due to increasing glacier melting, above Lago dei Seracchi (the blue dot in Figure 7.1 refers to the probe location). Figure 7.2 shows the probe position in the environment. A multiparametric probe has been im-

Figure 7.1: *Rutor marginal lake and probe location. Source: Google Earth, Glacier Lab PoliTo.*

mersed in the lake, measuring water temperature, the level and some electric parameters, directly related to the probe functioning.

Figure 7.2: *Photo representing the probe position and the lake and glacier environment (Source: Glacier Lab PoliTo - Tamea S.).*

7.1 Available data

7.1.1 Water temperature data

The period of time in which measurements have been performed goes from July, 20^{th} to September, 14^{th} 2021. Figures 7.3 and 7.4 show the recorded data of the lake water temperature and of the lake water level.
The mean, the median, and the variance of the two series has been calculated and the results are reported in Table 7.1.

Variable	Mean	Median	Variance
Water temperature [°C]	5.6	5.3	2.3
Water level [m]	0.611	0.613	0.022

Table 7.1: *Parameters of measured data series.*

7.1.2 Air temperature data

The idea of the model is to follow a deterministic approach, so that the air temperature and the water temperature can be related through bulk equations representing physical phenomena. Data about air temperature have been downloaded from the Portale of ARPA VdA [4]. Many meteorological stations are present in the area, as shown in Figure 7.5. To be consistent, in particular because the region is in a mountainous area, only 5 stations, nearer

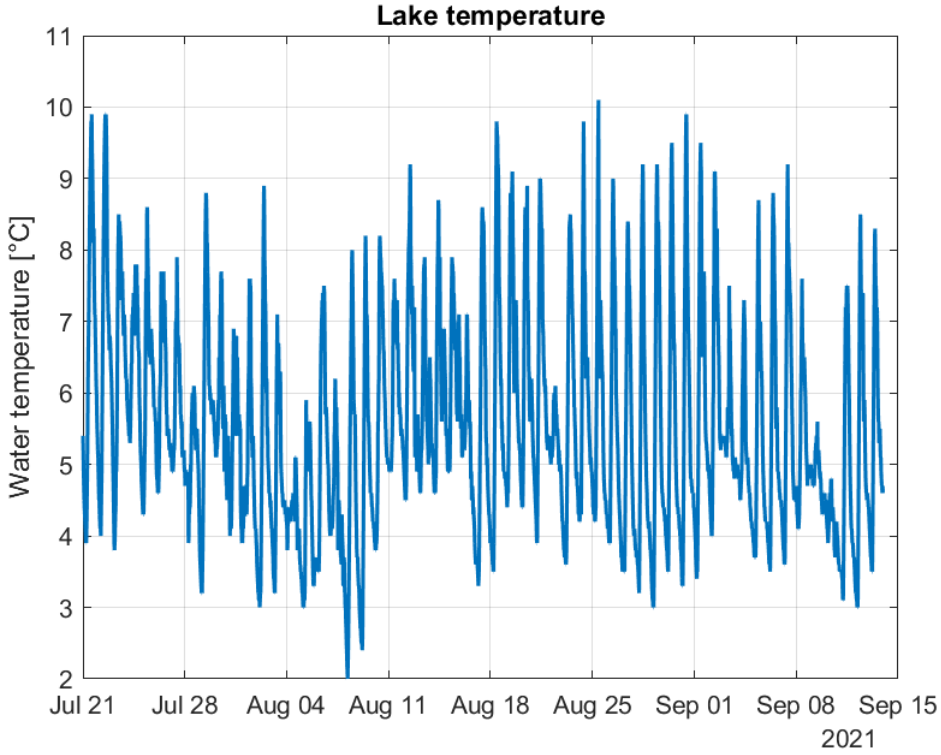

Figure 7.3: *Recorded data of lake temperature.*

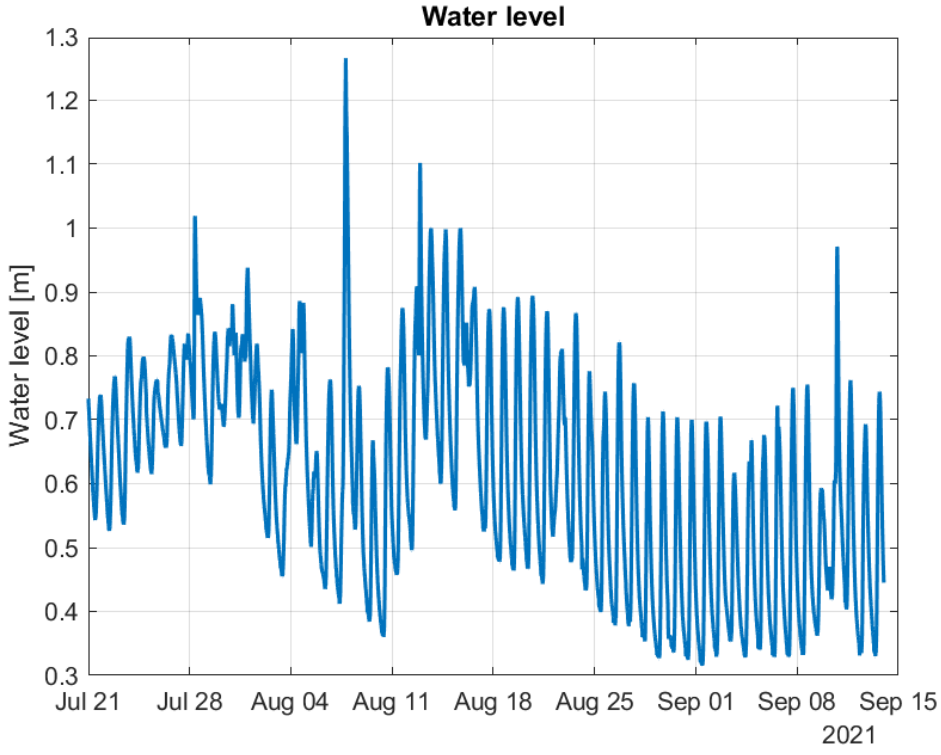

Figure 7.4: *Recorded data of water level.*

to the target, with different elevation have been considered (numbered in Figure 7.5). Data about air temperature in the chosen stations have been downloaded and analysed. Figure

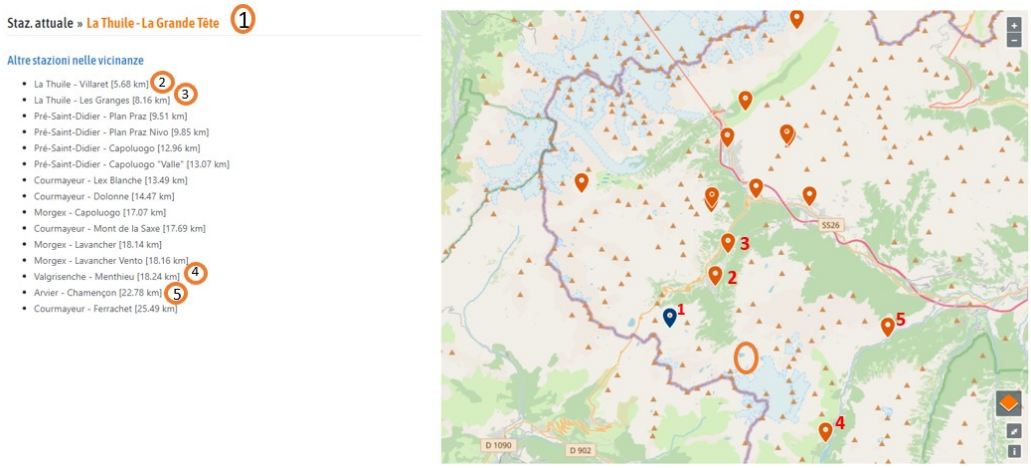

Figure 7.5: *Map showing the meteorological stations in the area. The red circle locates the target. Source [4].*

7.6 shows the air temperature and Figure 7.7 shows the precipitation at the different stations as function of time, in the considered period of year 2021. In Figure 7.6 it is visible how, increasing the altitude of the station, the temperature variability increases. Stations at lower elevation present higher air thermal excursion over the day and the night but more uniform distribution of the temperature along the period. As the elevation increases, the temperature oscillations among days is more pronounced. The difference in temperature between the maximum temperature reached during the day and the minimum one reached at night is lowers; all those factors have to be considered when estimating the temperature at an elevation that is higher than the ones covered by the meteorological stations.

Concerning precipitation amount, it can be observed from Figure 7.7 that, regardless from the elevation, the station located at Valgrisenche - Menthieu recorded an higher amount of rainfall in some of the occurred events, especially in the first part of the series. In Figure 7.7e it can be observed that the frequency of the rainfall events at this higher elevation station is not much larger, but the total amount of rainfall that reached the ground any time was on average larger that the other stations. This phenomenon can be due to the temperature series. This observed trend can be commented as the fact that the elevation can affect very much the weather, and in summer precipitation can occur as very local events; the intensity of the precipitation has to be considered as well when trying to model water runoff and thermal regime of water bodies. To sustain the thesis that the precipitation can vary very much locally, especially in summer months, and that it is not the driving factor for the water thermal regime estimation at the target, Figure 7.8 shows the water level of the small lake together with the precipitation at La Grand Tete station.

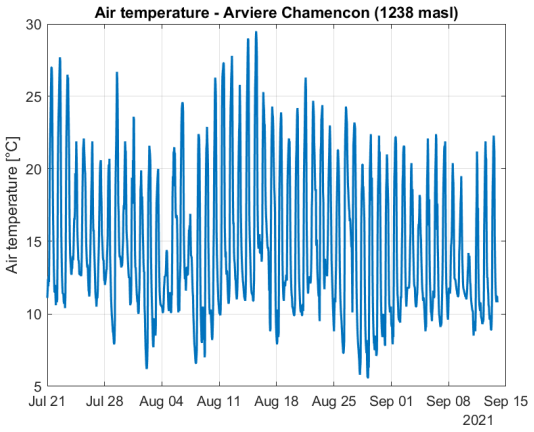

(a) *Arviere Chamençon, 1238 masl.*

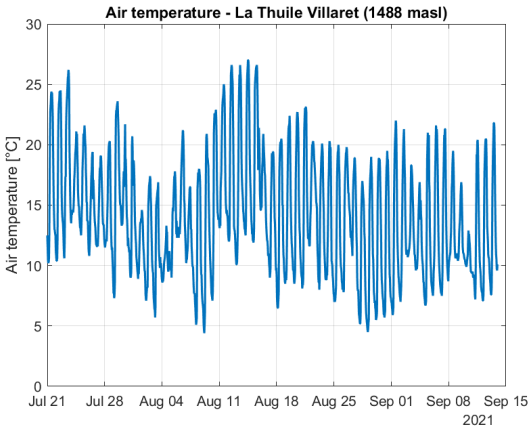

(b) *La Thuile - Villaret, 1488 masl.*

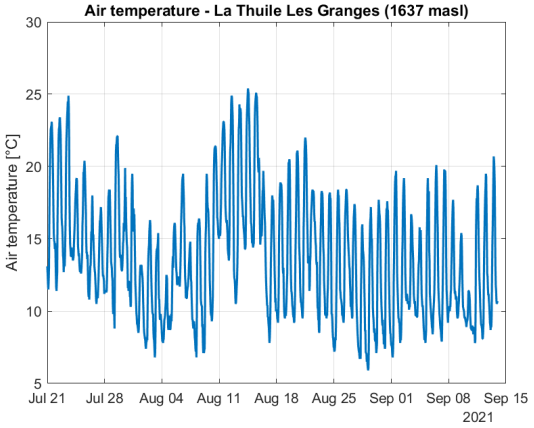

(c) *La Thuile - Les Granges, 1637 masl.*

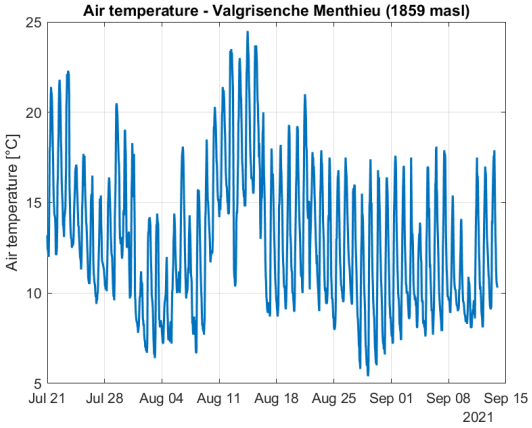

(d) *Valgrisenche - Menthieu, 1839 masl.*

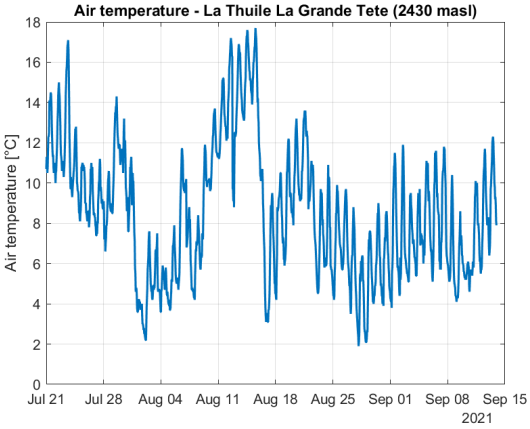

(e) *La Thuile - La Gran Tete, 2430 masl.*

Figure 7.6: *Air temperature at the different ARPA VdA stations.*

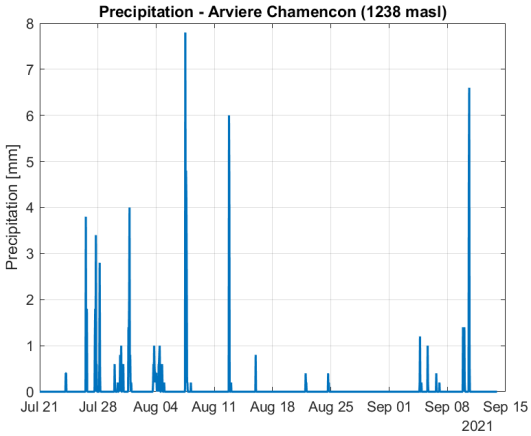

(a) *Arviere Chamençon, 1238 masl.*

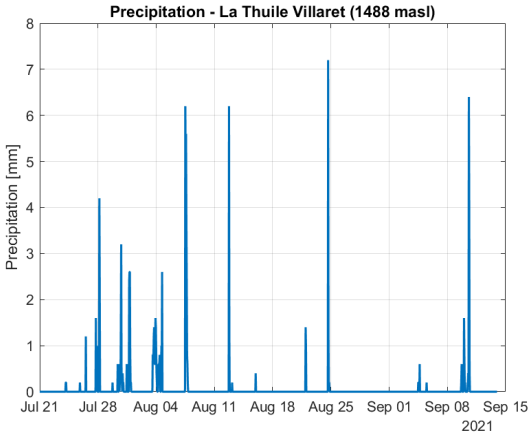

(b) *La Thuile - Villaret, 1488 masl.*

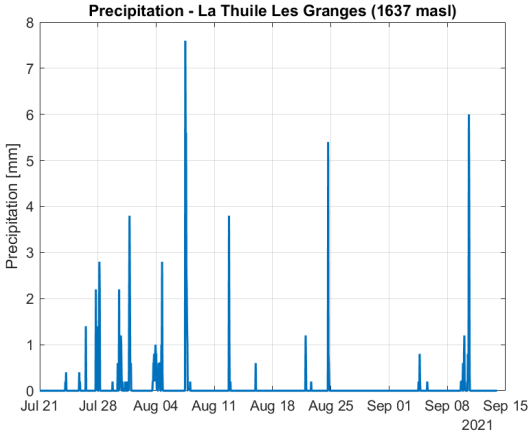

(c) *La Thuile - Les Granges, 1637 masl.*

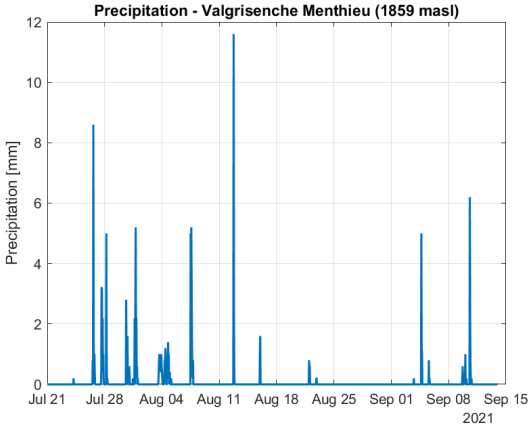

(d) *Valgrisenche - Menthieu, 1839 masl.*

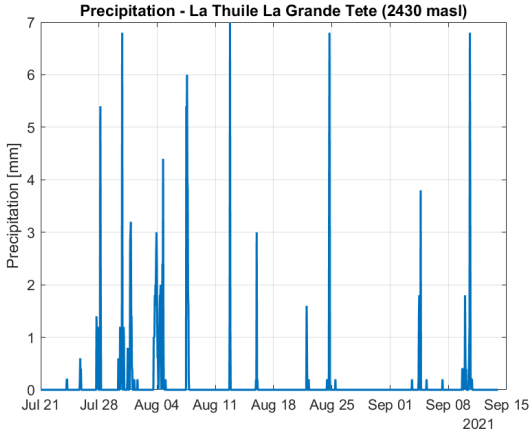

(e) *La Thuile - La Gran Tete, 2430 masl.*

Figure 7.7: *Precipitation at the different ARPA VdA stations.*

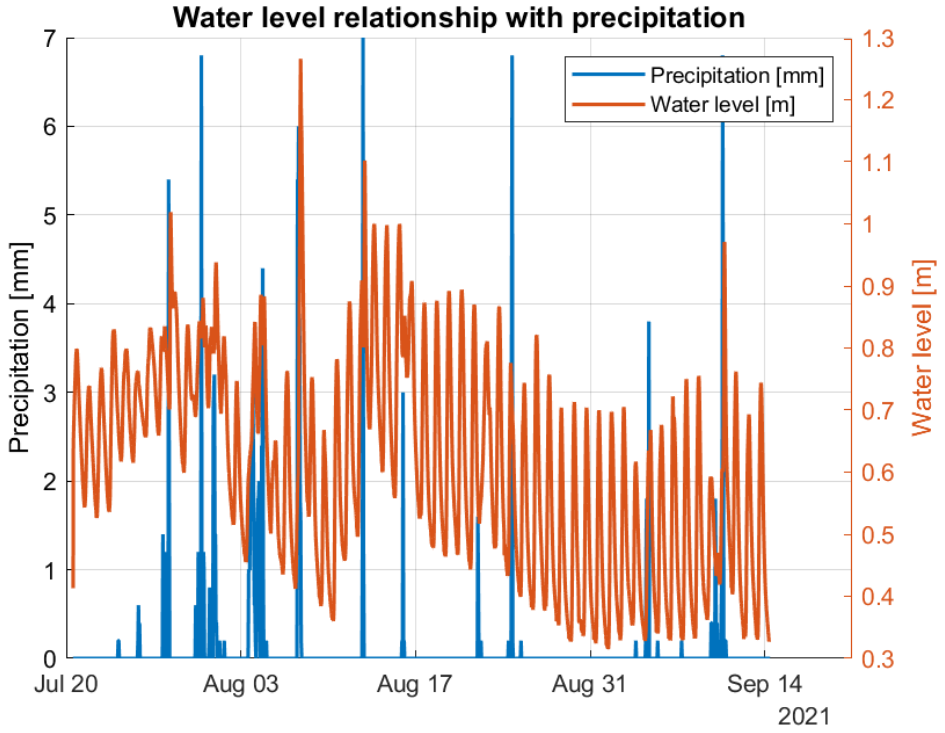

Figure 7.8: *Lake water level with precipitation time series at La Thuile - La Grand Tete.*

7.2 Temperature estimation

The next step is to estimate the air temperature at the target: having data from different stations at different elevations, it is possible to estimate an hourly lapse rate. Lapse rate is defined as the variation of the temperature with the height. In the Earth's troposphere, temperature declines with height, with an approximately linear behaviour

$$\Gamma = -\frac{\partial T}{\partial z} \tag{7.1}$$

where:
Γ Lapse rate [°C/m]
T Air temperature [°C]
z Elevation [m]
Data from 2002 to 2021 have been used to estimate a mean hourly lapse rate, as linear interpolation of the mean temperature with respect to the altitude as

$$T(z) = A \cdot z + B \tag{7.2}$$

where:
T Estimated temperature at a certain altitude [°C]

z Altitude [m]
A and B are the linear regression coefficient. Coefficient A represents the lapse rate and the intercept represents the mean temperature at the sea level ($z = 0\,\text{m}$) [4].

All the available (2002-2021) hourly data concerning the considered period (July 21^{st} - September 13^{th}) have been downloaded from the ARPA VdA portal. At first, a series of hourly values has been obtained, by averaging the data over all the available years, for every station. The obtained series has then been organised as a matrix where every column is a day of the specified period, and every row is an hour from 1 to 24. As further step the matrix has been averaged over the rows, so that a vector of 24 multi-day mean temperatures was obtained, for every station. Finally, every value of the five obtained vectors has been linked to its correspondent from the other stations and a linear regression relation has been established. The slope of the linear regression line found hourly represents the hourly seasonal lapse rate for the summer period in general. The variability over years have been tracked and represented in Figure 7.9.

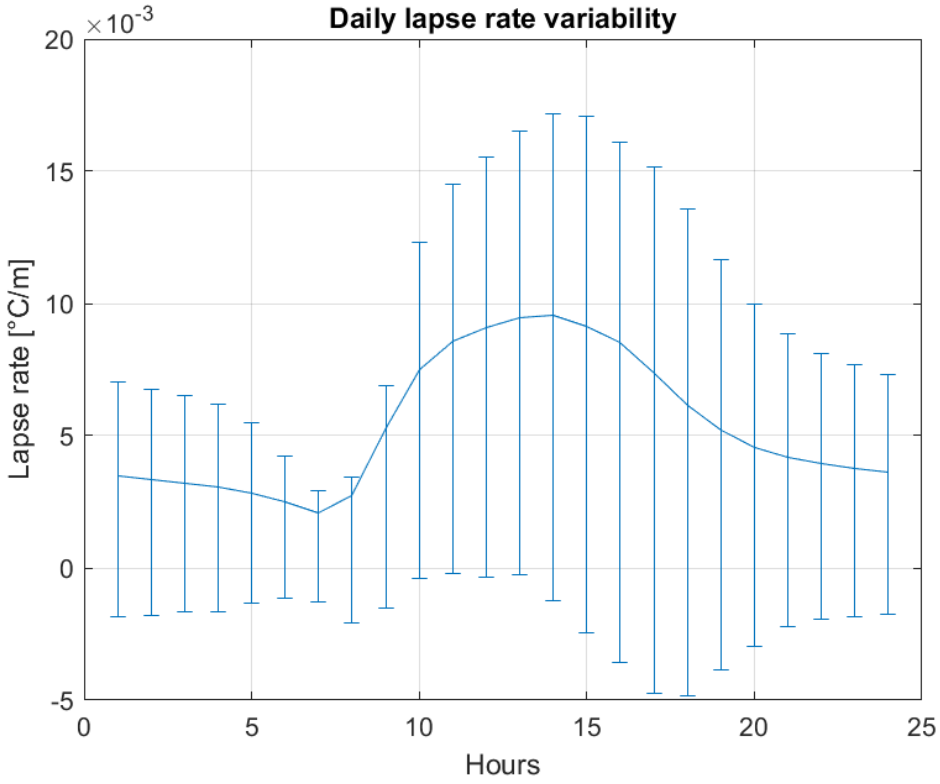

Figure 7.9: *Calculated lapse rate and its variability.*

As from the literature, typical values of lapse rate in the Alpine region, for the summer months are in the range of $0.6 - 0.65\,^{\circ}\text{C}/100\,\text{m}$. Rolland (2003), analysing the Alpine region, found an evident seasonal trend in the lapse rates, being the values higher in summer and lower in winter [38]. Looking at Figure 7.9, it can be noticed that the found values are

compliant with the one found by Rolland (2003). Night values are expected to be slightly lower, due to the behaviour of the atmospheric boundary layer. To be noticed, in addition, the wide variability of the hourly lapse rate. The wide variability is consistent with the literature [38] [18]. Once got the lapse rate, the altitude of the target is needed for the temperature estimation. The estimation of the altitude of the lake has been done using the exact coordinates of the probe, georeferenced coordinates.

In Figure it is represented the altitude of the lake that has been measured during the measuring campaign. The altitude of the lake is 2504 m asl.

To estimate the temperature at the lake location, the temperature of every station, at any hour for the all analysed period, has been corrected, according to the calculated hourly lapse rate. The temperature difference with respect to the target elevation has been calculated for every station at any time in the series. Once the temperature corrections at all the five stations have been evaluated, the average of the results, at any time of the series, is computed. The average temperature is assumed to be a new estimation of the air temperature at the lake elevation. Doing such a reasoning means correcting every value of the temperature series, at any station, by a constant value, that depends on the difference in elevation between the considered station and the target elevation. In general, a constant correction can be applied at the mean temperature series among all the considered station, by multiplying the hourly lapse rate by the difference between the mean elevation of the stations and the lake elevation:

$$T(z_{lake}) = \Gamma\,(z_{lake} - \overline{z}) + \overline{T} \tag{7.3}$$

where:
z_{lake} Lake elevation [m]
$\overline{z}$ Mean station elevation [m]
$\overline{T}$ Mean station temperature [°C]

In Figure 7.10 it is shown the hourly correction applied to the mean temperature series. The correction is negative because the lake elevation is higher with respect to the stations mean elevation, thus the estimated temperature at the lake is expected to be lower than the mean temperature of the stations. In Figure 7.11 the estimated temperatures with the above cited correction method and the temperatures recorded at La Grand Tete station are represented. From Figure 7.11 it is consistent that the temperature is in general similar or a bit lower than the one measured at the station, since the target location is an higher elevation with respect to La Grand Tete station.

To check the consistency of the method, also the temperature at each station, starting

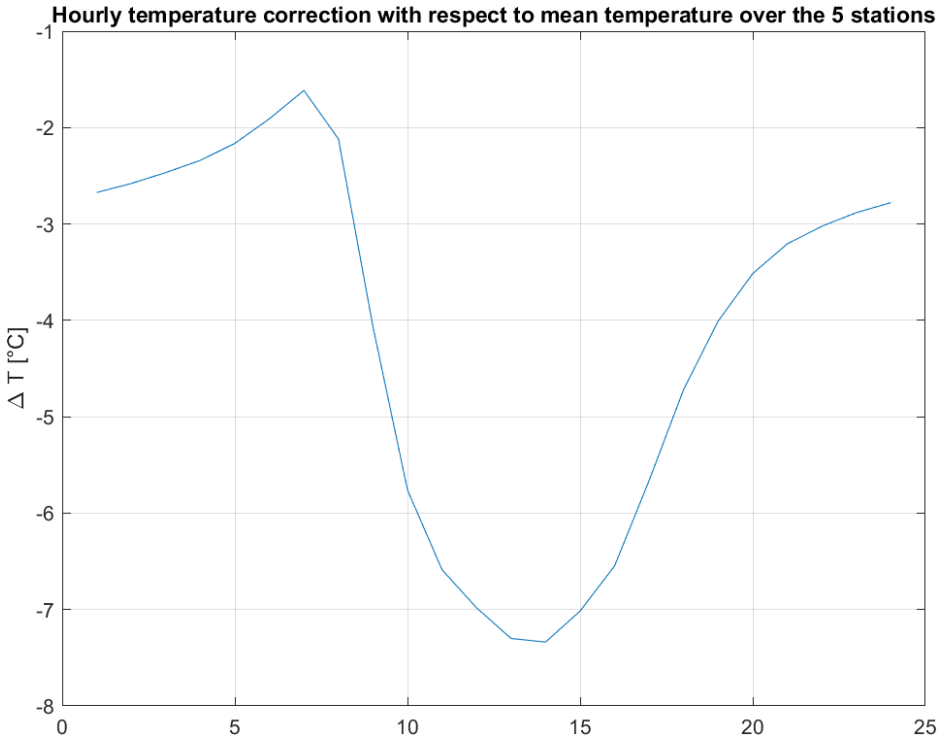

Figure 7.10: *Hourly temperature correction applied to the mean temperature over the 5 available stations.*

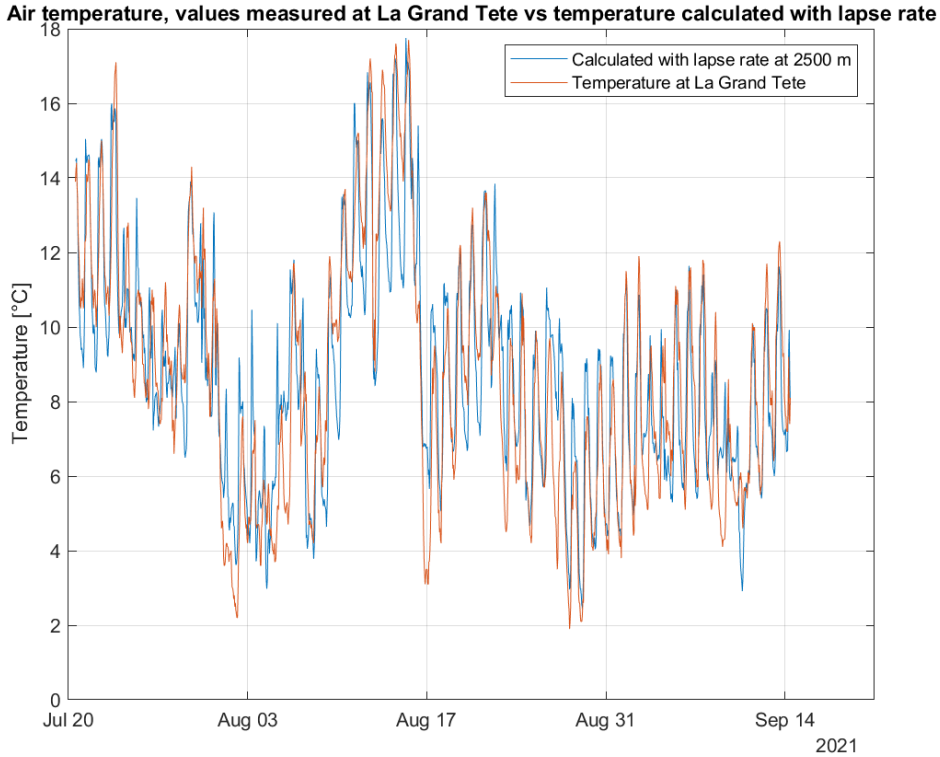

Figure 7.11: *Temperature calculated with corrections at the lake and temperature measure at La Grand Tete station.*

from the temperature recorded at the other available stations has been calculated. In Figure 7.12, the temperature estimated at La Gran Tete station is represented, together with the recorded series at that station. It can be observed that in general the trend and the amplitude of the peaks is respected. Some more differences are shown in correspondence to rainy days, where humidity plays a big role in affecting air temperature.

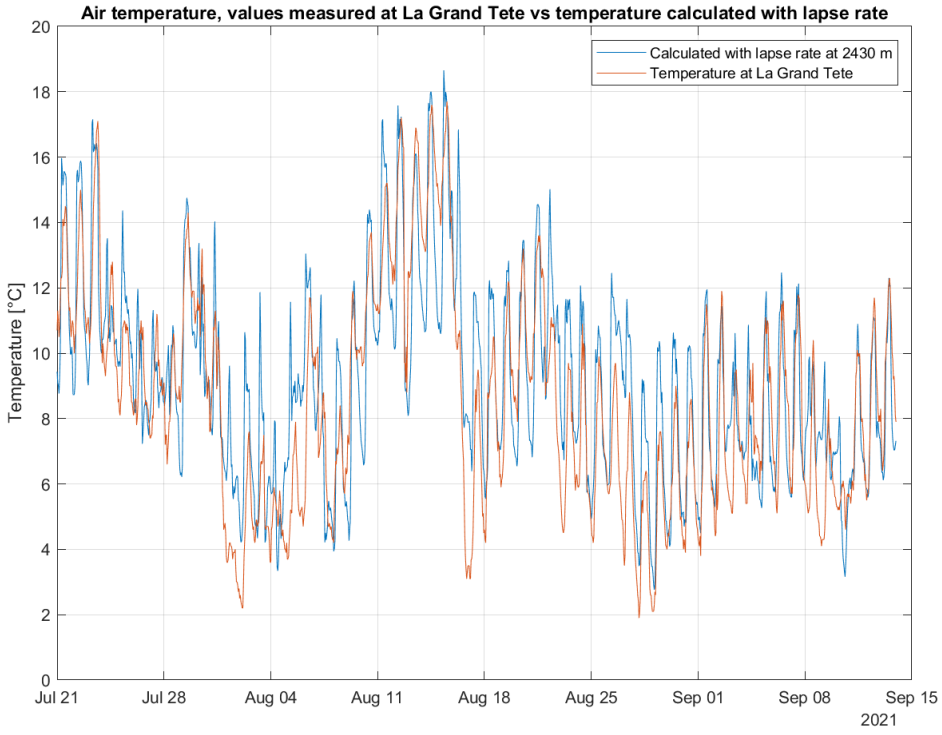

Figure 7.12: *Temperature calculated with corrections and temperature measure at La Grand Tete station.*

One of the main problem can be that air temperature changes do not only depend on elevation. Geographic and topographic variables play a fundamental role in air temperature estimation. Observed near surface lapse rate can can be affected by topography, and other atmospheric parameters such as air humidity, wind speed and wind direction, cloud cover, and radiative conditions [32]. In addition, large variability has been found when considering either the maximum or the minimum or the mean temperature. High seasonal variability has been noticed [18].

7.3 Pressure estimation

To estimate more data and have a more complete set of characteristics in time of the observed target, also the time of the atmospheric pressure have to be estimated. An hydrostatic balance can be constructed as simple assumption of the atmosphere equilibrium of forces.

The vertical forces acting in the atmosphere are gravity and the pressure gradient. Gravity force pulls the air molecules toward the center of the planet, while the pressure gradient is opposite, pushing molecules towards the outer atmosphere. If the forces are considered to be in balance, the Equation 7.4 of hydrostatic balance per unit mass can be assumed to hold:

$$g = -\frac{1}{\rho}\frac{dp}{dz} \tag{7.4}$$

For sake of simplicity, ideal gas equation can be assumed to hold in this case (Equation 7.5, where R is the ideal gas constant).

$$p = \rho RT \tag{7.5}$$

Substituting Eq. 7.5 into Eq. 7.4, with some rearrangements one gets

$$\frac{dp}{p} = -\frac{dz}{H} \qquad \text{where} \qquad H = \frac{RT}{g} \tag{7.6}$$

where H is referred as to scale height. If the atmosphere is assumed to be isothermal, the pressure at any height z can be retrieved from the integration of Equation 7.6 as

$$p(z) = p_s e^{-\frac{z}{H}} \tag{7.7}$$

where p_s is the atmospheric pressure at the sea level.
From Equation 7.7, for an isothermal atmosphere, the pressure decreases by e^{-1} every scale height. The scale height for the mean temperature of the Earth's atmosphere is 47.6 km [23]. Taking this as a good theoretical assumption, an empirical scale height has been estimated and compared to it. Data have been downloaded from the ARPA VdA website [4], considering 9 stations around the target, with different elevation, for 17 years long (2005-2021). Using an analogous reasoning to the one for lapse rate calculation, the hourly scale height that can be applied for the whole period of the series has been evaluated. The natural logarithm of the pressure series have been interpolated as linear in height, to get the hourly scale height:

$$\ln\frac{p(z)}{p_s} = -\frac{z}{H} \qquad \rightarrow \qquad \ln p(z) = -\frac{1}{H}z + \ln p_s \tag{7.8}$$

Thus, a linear relation is established between the natural logarithm of the pressure and the height at which it is measured. The slope of the line is the scale height. In this way an analogous estimation process to the lapse rate in the previous section is justified. In Figure 7.13 it is represented the result of the interpolation. As for the lapse rate used for the temperature estimation, the correction to be applied hourly to the mean pressure, to get the atmospheric pressure at the lake has been evaluated. Figure 7.14 shows the result to be applied as correction to the mean pressure to the the target pressure. Once got the empirical scale height, the

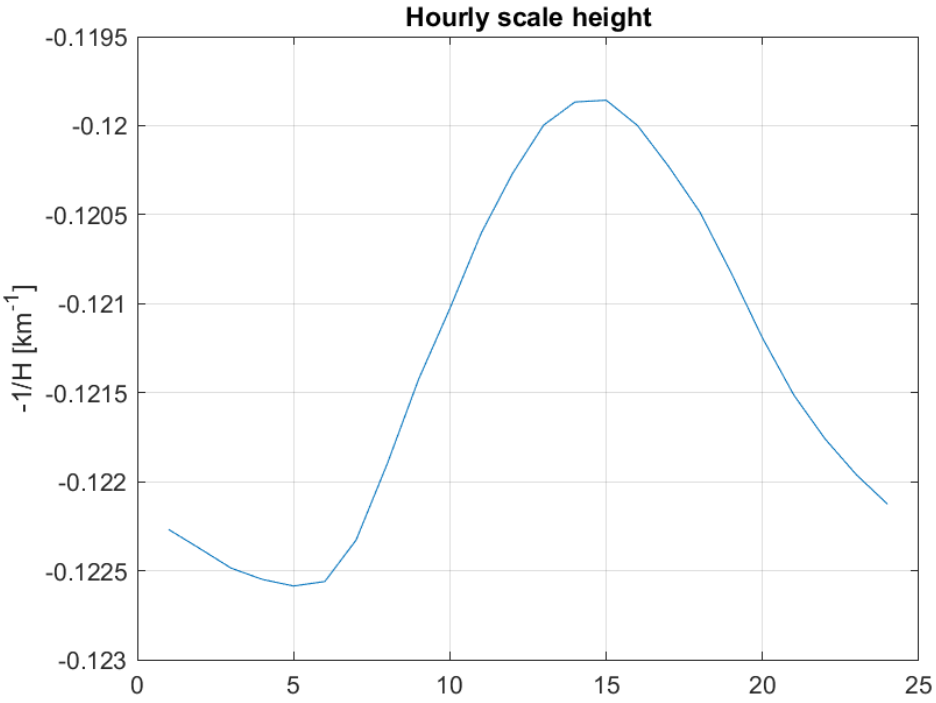

Figure 7.13: *Hourly scale height series.*

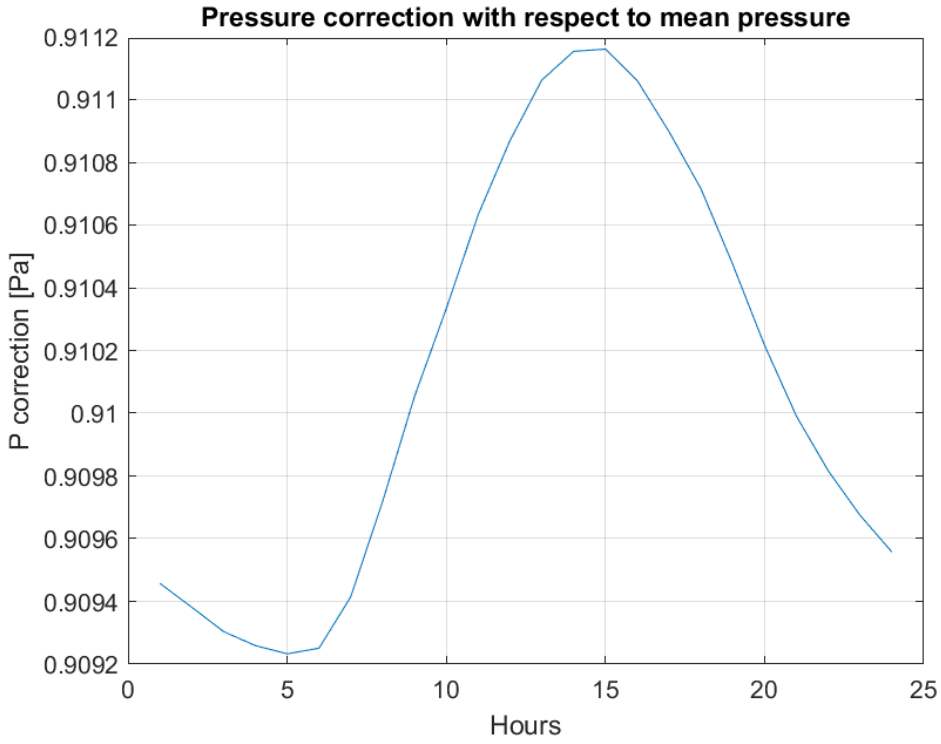

Figure 7.14: *Hourly correction to be applied to the mean atmospheric pressure.*

pressure at the altitude of the target has been estimated, and compared with the constant estimation from the theoretical scale height ($H = 7.6\,\text{km}$). Figure 7.15 shows the result. What can be observed from Figure 7.15, is that, in general, the pressure is higher in the empirical

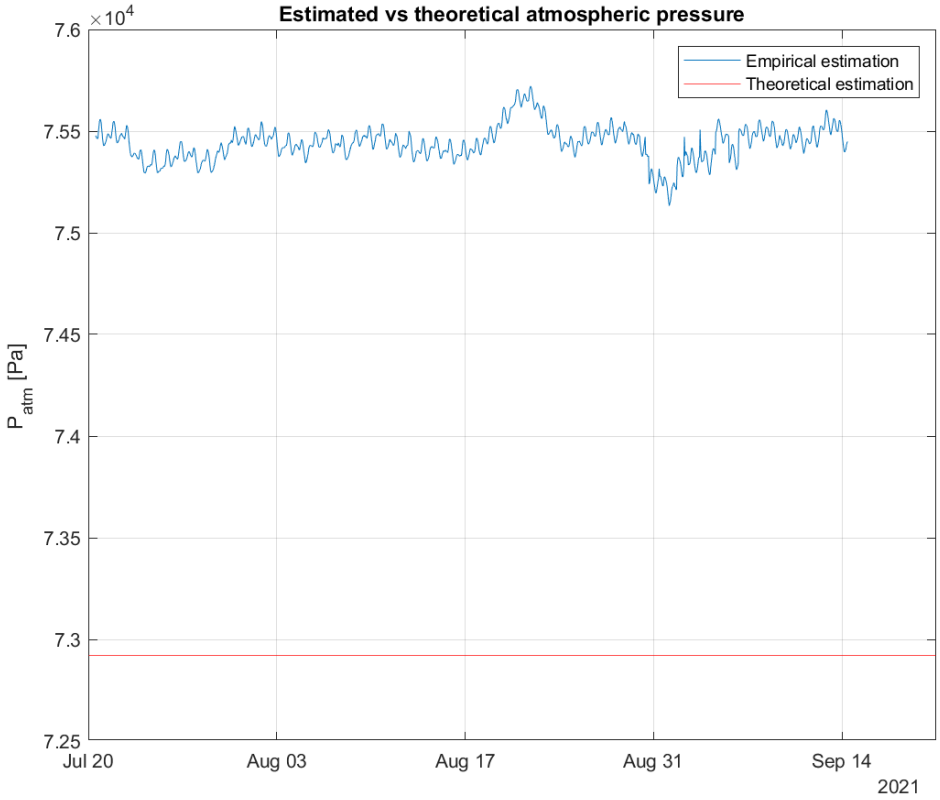

Figure 7.15: *Hourly atmospheric pressure, empirical and theoretical estimation.*

estimation with respect to the theoretical estimation and the rate of variability is not wide. The difference between the two estimations can be mainly due to changing weather and to the orography/topography of the site.

7.4 Lake and air temperature correlation

When performing statistical data analysis, it is worth verifying the eventual link between the involved series. The two series that have to be compared are the lake water temperature series and the air temperature, estimated at the height of the target. As a first statistical analysis of the data the cross-correlation of the residuals of the two series is plotted in Figure 7.16. Then, autocorrelation of the two separated series is evaluated (Figure 7.17 and 7.18). Looking at the two graphs in Figure 7.17 and 7.18, it can be observed that the two curves show, as expected, a similar behaviour: the sinusoidal behaviour is present in both plots. The lags are one hour long. As expected, after two days the data are almost no more autocorrelated. This trend means, reasonably, that if one has the temperatures series of the day before, the temperatures of the day after can be predicted with a certain uncertainty, but they can be considered acceptable. Going further with the time lag the temperature prediction relying on the temperatures of some days before are no more consistent.

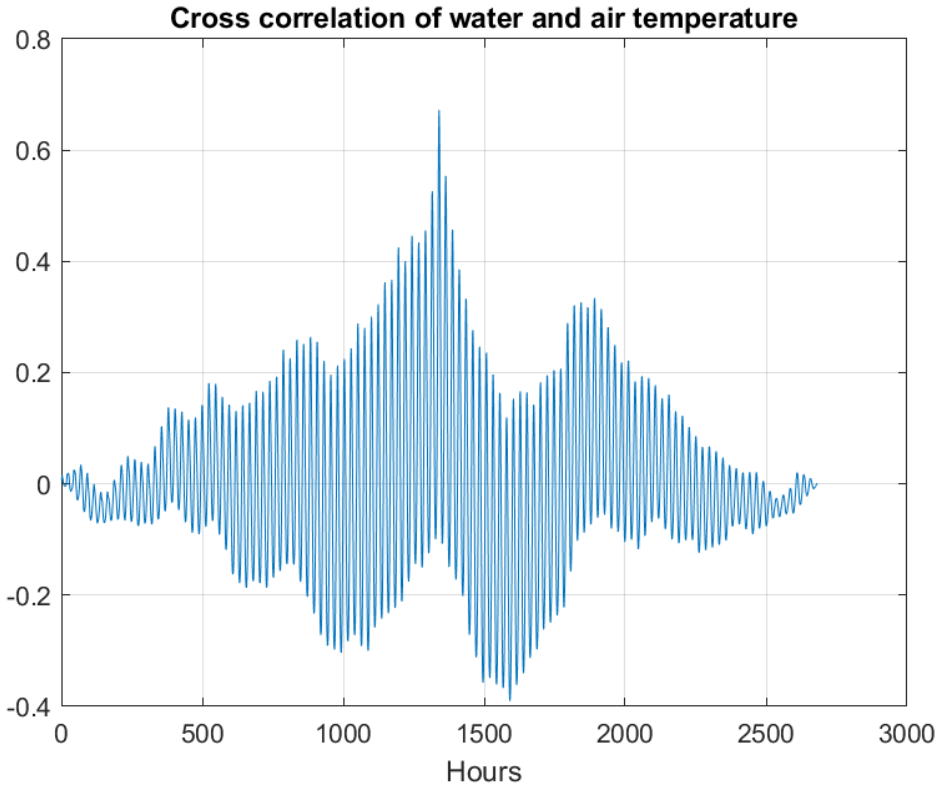

Figure 7.16: *Cross-correlation of residuals of air temperature at lake site and lake water temperature.*

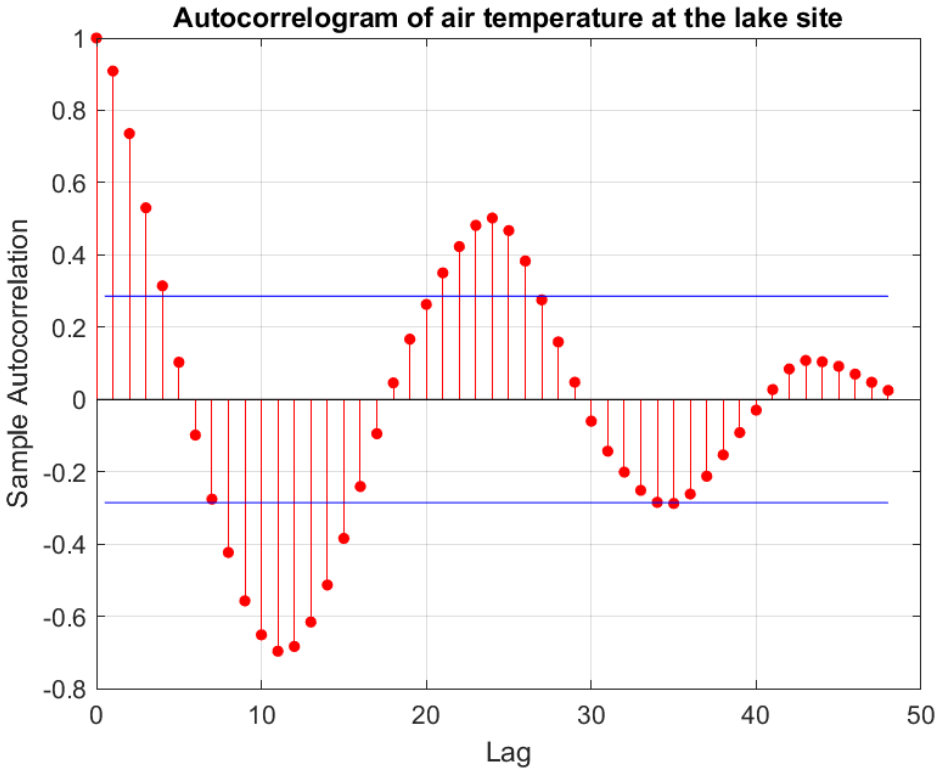

Figure 7.17: *Autocorrelogram of mean daily air temperature at lake site.*

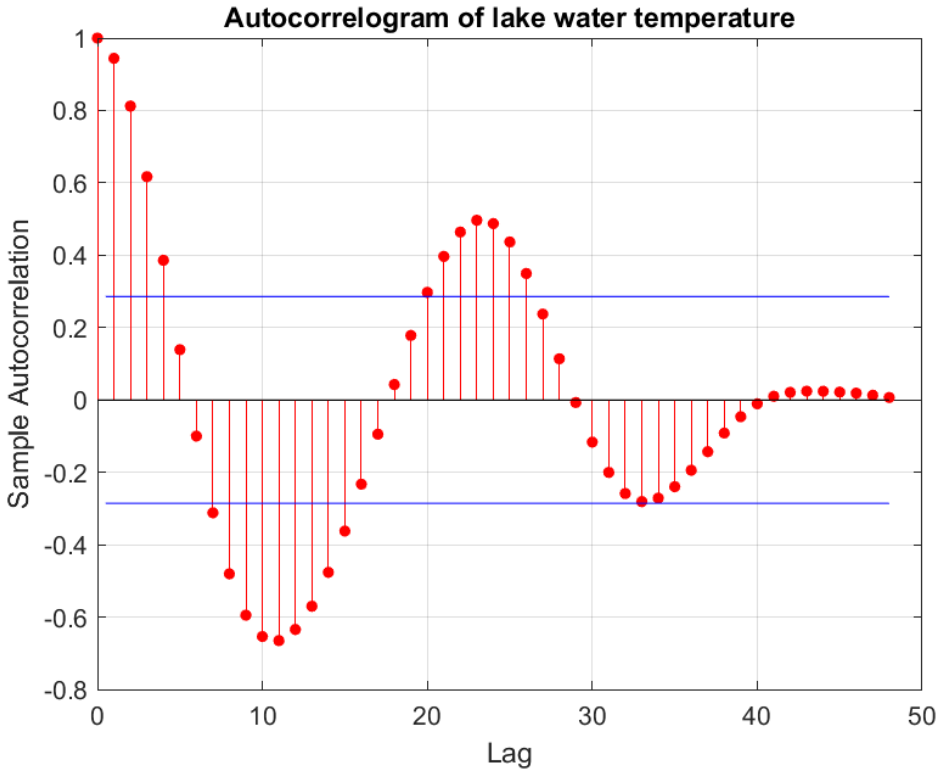

Figure 7.18: *Autocorrelogram of mean daily lake water temperature.*

As a general hypothesis, due to the different thermal capacity of the two media, there can be a delay in the water temperature with respect to the air temperature [28]. The cross correlation of the two series has been calculated by shifting any time by one Δt ($\Delta t = 1$h) the air series, with respect to the lake temperature series. 24 curves have been obtained, showing a delay of at most five hours of the water temperature with respect to air temperature. For a better visualisation of the phenomenon, a map of the crosscorrelation coefficient (normalized), showing the behaviour of the water temperature series with respect to the shifted air temperature series have been plotted (Figure 7.19).

From Figure 7.19 it can be observed that:

- In the first hours of the day water takes less time to warm up, due to its thermal capacity that kept the heat from the day before.
- As soon as the sun starts to directly irradiate that portion of atmosphere, a delay is observed in the water temperature with respect to air temperature to increase, due to water thermal inertia.
- In the middle of the day the delay is slightly lower and can be considered almost symmetric.

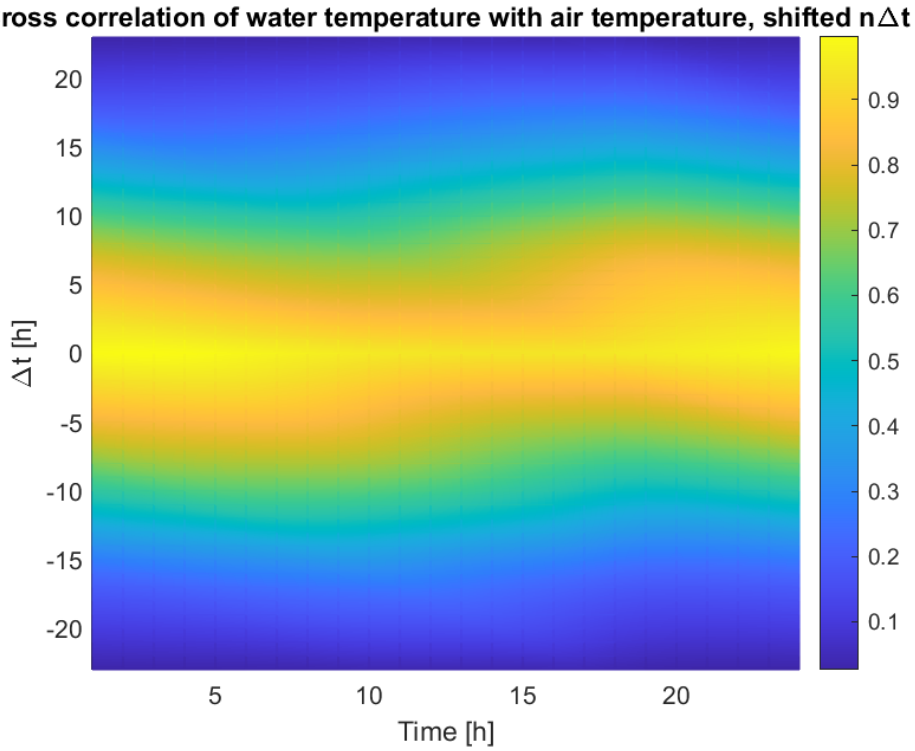

Figure 7.19: *Crosscorrelation map between air and water daily temperature.*

- In the early afternoon the air starts cooling down as the sun radiation changes its angle, whereas water keeps the heat gained until then, thanks to its thermal capacity.
- The situation is the same until night, even if its entity is slightly attenuated, until the morning.

From Figure 7.20 it is well visible the difference at the early morning and in the late afternoon as commented above. Every day the cycle is similar, the cycle shown in the maps has been obtained from an average of air and lake temperatures, over the considered period. What is worth noticing is how important is the presence of the mixed layer in the atmospheric boundary layer, due to sun direct radiation. Sun irradiance changes significantly air temperature near the ground, and this in turn affects water temperature. The considered period is the more critical one for glaciers, especially in recent years, when climate changes started to present more tangible effects. During summer months direct solar irradiance causes ice melting, from which arrives the main part of water filling the target lake.

In Figure 7.21 it is shown the difference between air temperature estimated at the lake site and the lake water temperature, as an average on the whole period. The difference has been calculated by subtracting the lake temperature from the air temperature. This means that the air is always warmer that the water, also at night, not exactly what would have

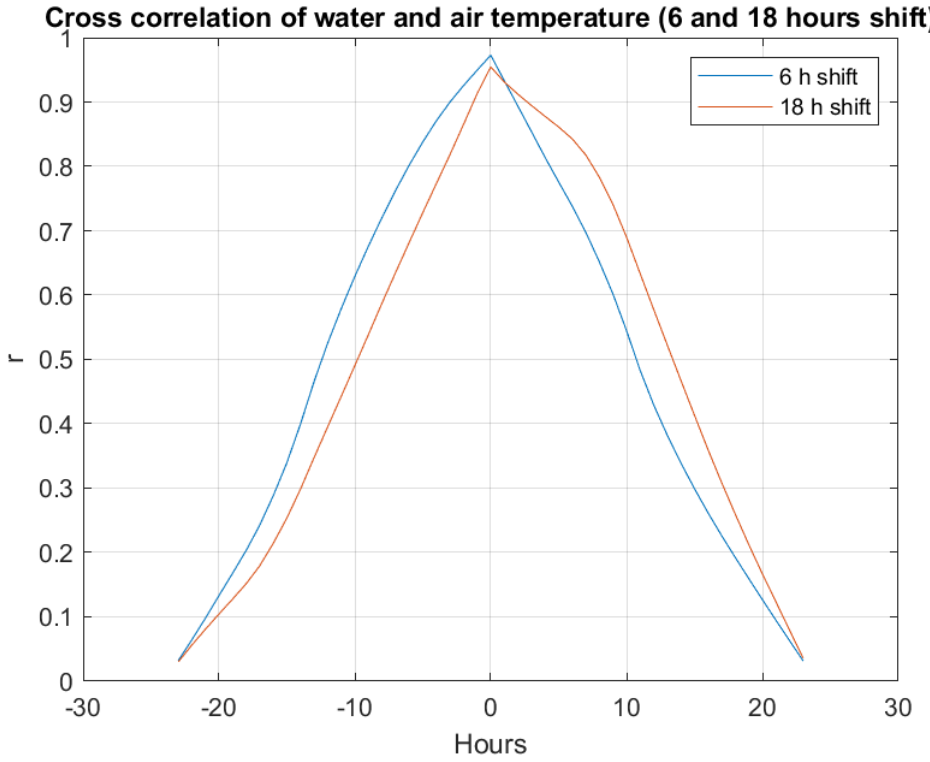

Figure 7.20: *Crosscorrelation between air and water daily temperature with 6 and 18 hours shift.*

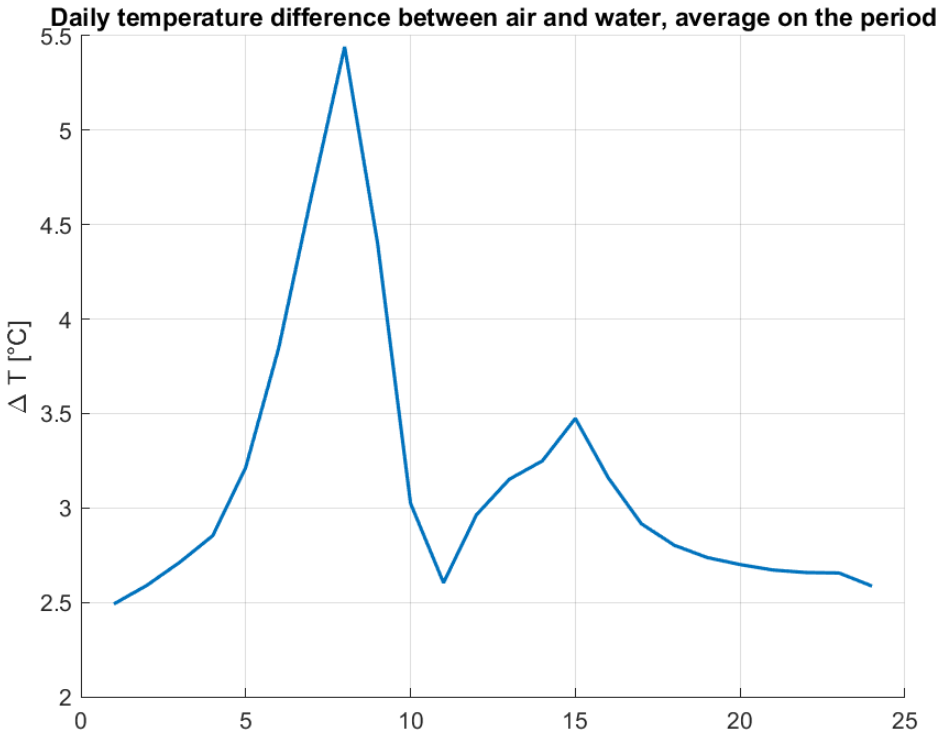

Figure 7.21: *Average air and water temperature difference.*

been expected. This happens probably because of the summer season. A general trend in

the plot can be noticed: the minimum difference in temperature can be observed in the late morning/mid day hours, time interval in which also the crosscorrelation plot (Figure 7.19) shows the least delay between the two variables. Before averaging the the data obtain the curve in Figure 7.21, a curve per day has been plotted. A certain variability among days can be noticed, but it would be an acceptable behaviour, considering the large number of variables affecting both water and air temperature (e.g., clouds, air humidity, wind velocity and direction, rainfall). Only few days show negative difference, in morning hours. These days are days in which precipitation occurred.

To assess the relation between air and water temperature a first simple trial of linear regression between the two variables has been computed. The result is shown in Figure 7.22. To estimate the the goodness of the fit of the linear regression line, the coefficient of

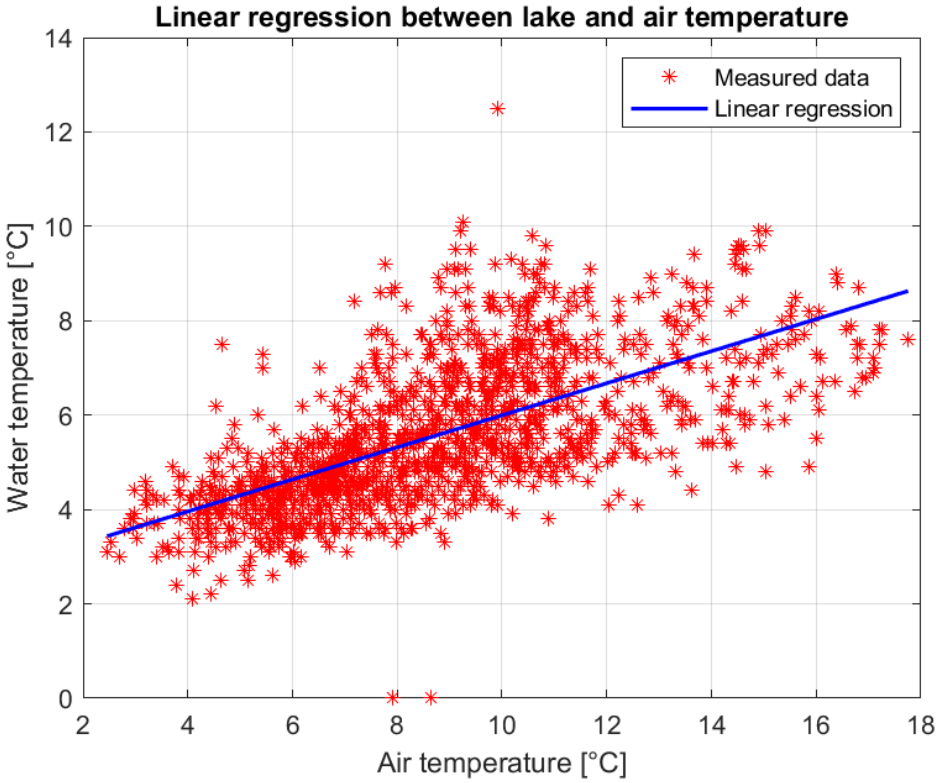

Figure 7.22: *Linear regression between water and air temperature.*

determination R^2 has been calculated as

$$R = 0.4217 \tag{7.9}$$

This means that the linearly interpolated line can predict only the 42% of the variance in the water temperature series.

8. Model construction

The objective of the work is to write a model for the calculation of the water temperature of the Rutor marginal lake, from the air temperature. The temperature of the lake have been measured with an half an hour interval from July, 20^{th} to September, 14^{th} 2021.

Given the relatively small available data for the model computation, a deterministic model, based on energy balance have been chosen as method to achieve the objective of the work. The change in water temperature in a point of a channel, due to thermal fluxes, can be expressed as:

$$\frac{\partial T_w}{\partial t} = -U\frac{\partial T_w}{\partial x} + D_L\frac{\partial^2 T_w}{\partial x^2} + \frac{\Delta H}{\rho c_p d} \tag{8.1}$$

where:
T_w Water temperature [°C]
U Mean channel velocity [m/s]
D_L Longitudinal dispersion coefficient [m/s^2]
ΔH Total energy balance [W/m^2]
ρ Water density [Kg/m^3]
c_p Specific heat of water [J/Kg °C]
d Channel depth [m]
Eq. 8.1 is referred to a channel. Since it is used for the calculation of temperature variation in time in a point, it is compliant with the objective of the work.

The model, for sake of completeness wants to get a measure of the temperature of the whole lake. To do so, Eq. 8.1 has to be integrated on the total lake surface. Computing the integral, the depth d, in this case of the lake, becomes the mean depth of the lake $\overline{d}$. This happens because when integrating, the whole lake volume is considered. When moving at the denominator of the right side of the equation the thermal capacity term, to isolate the temperature, area of the lake cancels out in the last factor (ΔH factor). So what is important to notice is the change in the d conceptual quantity.

8.1 Advective term

The advective term, when integrating on the whole lake, is composed only by the entering thermal flux at the lake inlet and by the exiting flux at the lake outlet, because all other factors vanish. What is important to assess is the entity of the two fluxes. If the two fluxes can be considered very similar between them, then it can be assumed that the error that arises by neglecting this term is very small. The considered lake is a small one, seasonal one, thus it can be assumed that the thermal difference at the inlet and at outlet of the lake is negligible.

8.2 Diffusive term

Concerning the diffusive term, where the second spatial derivative appears, when integrating on the whole lake, it cancels out if adiabatic boundaries are assumed. Even though for sure a certain heat exchange is present between the lake water and its boundaries, since the groundwater and the riverbed contributions to the total heat exchange is going to be neglected, it is reasonable to assume adiabatic boundary conditions.

8.3 Heat exchange

The most important term of Eq. 8.1 for the objective of this work is the energy term. As theoretically explained in section 6, there are many different contribution to the heat exchange occurring at the surface between water and air. All those contributions can affect water temperature variations, with a different weight. When integrating the equation, the energy flux is multiplied by the area of the lake. When isolating the water temperature on the left handside, the area of the lake at the numerator simplifies with the area composing the volume at the denominator, leaving the mean depth of the lake $\overline{d}$ at the denominator. In the following every component of the total energy flux exchanged is carefully evaluated.

8.3.1 Shortwave radiation

To calculate the shortwave radiative flux contribution, the radiation registered by the instrument at the station located in La Thuile - La Grand Tete is used. The data have been assumed to be consistent since the station is located at an elevation comparable with the target location, and it is the nearest station in the surrounding area. In addition no other data are available, thus, in order to avoid further computational errors, the data series of La Grand Tete has been assumed to be reasonable.

The albedo coefficient for water has been retrieved from the literature [23] [15], in absence of significant images from where estimate it from. Albedo coefficients for water are between 0.05 and 0.12, depending on temperature, elevation and water turbidity [23]. Being the lake a small one, seasonal one, due to its glacial formation, it contains a lo of suspended sediments; for these reasons water has a quite high turbidity, that increases the albedo. Cogley (1979) [15] proposed to calculate the albedo for water in a different way, letting it depending on latitude (incident angle of the radiation) and month of the year. The proposed values from this work are tabulated by moth of the year and by latitude. Two different algorithms have been used: Fresnel method is less sensitive to diffuse radiation, while Grishchenko computation is accounting for diffuse component of the radiation. Considering the summer period, water albedo calculated by Cogley (1979) [15] in the two ways for the considered latitude, results higher with the Grishchenko method than with the Fresnel method. The albedo for water in summer season at the considered latitude must be in the range of 25% (at noon, maximum) to 4% (at the sunrise, sunset). A reasonable albedo coefficient assumption can be $\alpha = 0.07$ [15].
The net shortwave radiation affecting lake water temperature has been calculated from

$$H_{sw} = R(1-\alpha) \tag{8.2}$$

Since the measured radiation (R) is included in Eq. 8.2, it is expected to present a day night cycle. The time series of net shortwave radiative flux obtained is plotted in Figure 8.1. As

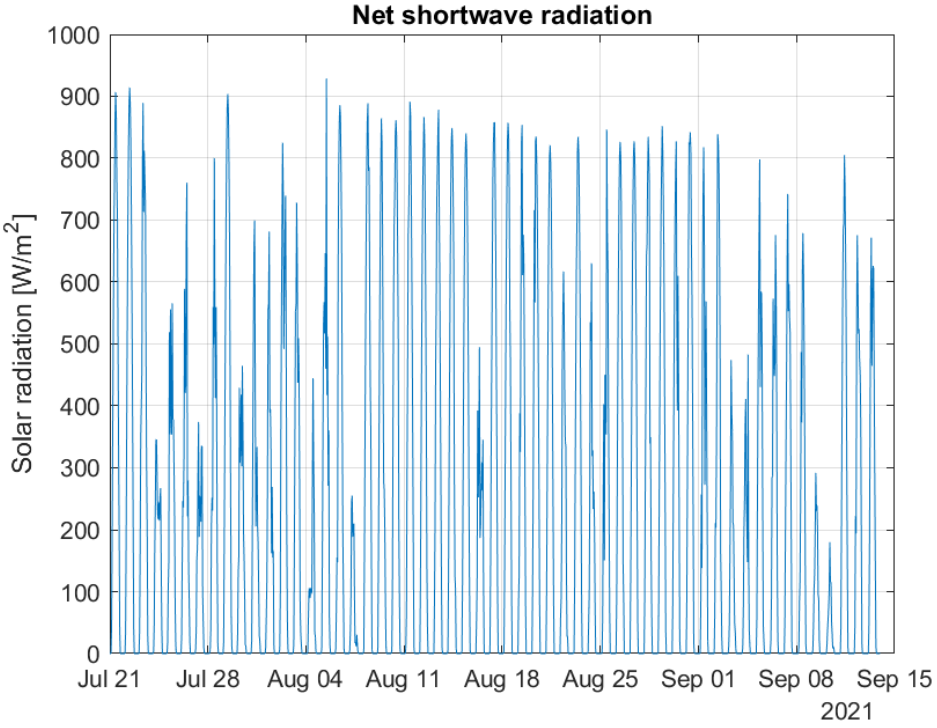

Figure 8.1: *Net shortwave radiation flux.*

expected, the night-day cycle is well visible and the values are on average compliant with the literature.

8.3.2 Longwave radiation

Longwave radiation radiative flux is a very important component of thermal balance of the lake. In magnitude, it gives a smaller contribution with respect to the shortwave radiation, but it is still very important because it depends on the lake temperature itself. The net longwave heat flux is estimated as

$$H_{lw} = \varepsilon_m C^b \sigma T_a^4 - \varepsilon_w \sigma T_w^4 \tag{8.3}$$

The first term in Eq. 8.3 refers to the incoming longwave radiation. The sky emissivity ε_m has an average value of 0.7, compliant with the literature [24] [11], as calculated from equation in Section 6.2. Since no data about the cloud cover in the area were available, a mean C value from the European model ERA-Interim has been assumed to be reasonable for the solution. In particular, $C = 0.3$ has been used for the computation, it has been retrieved from Figure 8.2. b has a value of -0.0227 [36]. Numerically, the cloud cover contribution reaches a value near to 1, not influencing that much the value of the longwave downward radiative flux. When comparing the cloud forcing factor with other data measured in North western Italian Alps, a positive forcing when the cloud cover increases is found. In general, it means that more clouds trap a bigger amount of thermal radiation that warms up the lower atmosphere, increasing the air temperature near the surface. In summer, at similar elevation, forcings of +20 W/m^2 to +60 W/m^2 have been measured in other locations of North western Italian Alps. of course the cloud cover influences, with a negative forcing though, the shortwave radiative flux as well. The absolute value of the cloud forcing that have been measured in comparable locations is higher for shortwave than for longwave radiation (mean value during the summer period). The net cloud forcing during the summer period is thus negative on average, with a quite strong dependance on the altitude of the site. Of course, it is important to consider all the factors (such as topography, vegetation, shading) influencing such values [31] [27].
Water emissivity has been assumed as $\varepsilon_w = 0.99$ [23]. Substituting such constants into the above equation, a series of the net longwave radiation it is obtained (Figure 8.3).

Observing Figure 8.3, it can be noticed that the night day cycle is not as pronounced as in the shortwave radiation graph. This is due to the already discussed shift in time of the water and the air temperature. Due to the dependence on water temperature, the longwave heat flux is affected by the presence of precipitation and the melting rate of the above glacier.

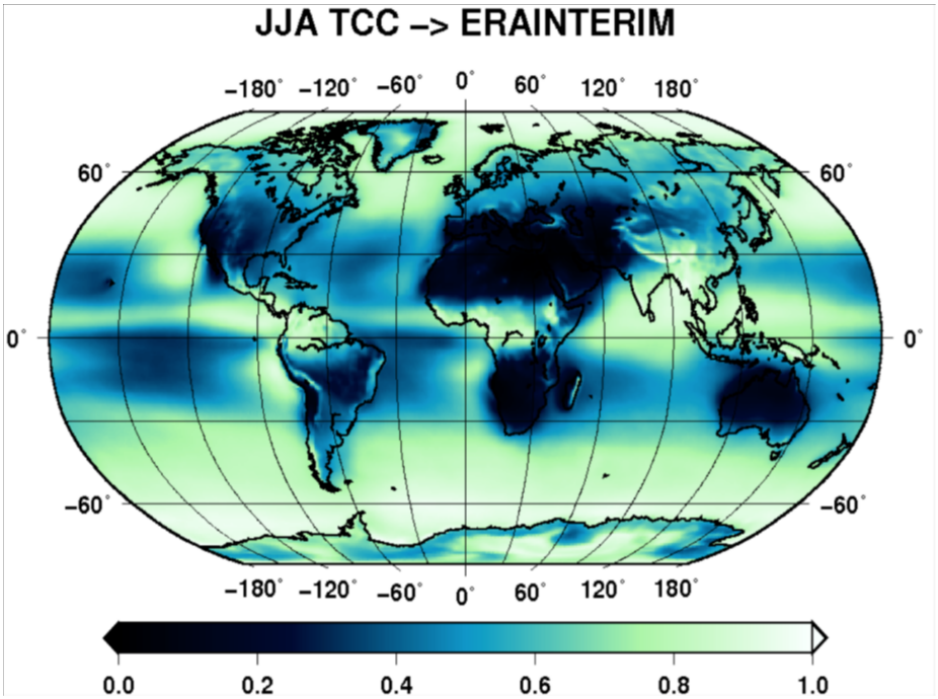

Figure 8.2: *Total cloud cover in the summer period from ERA Interim [22].*

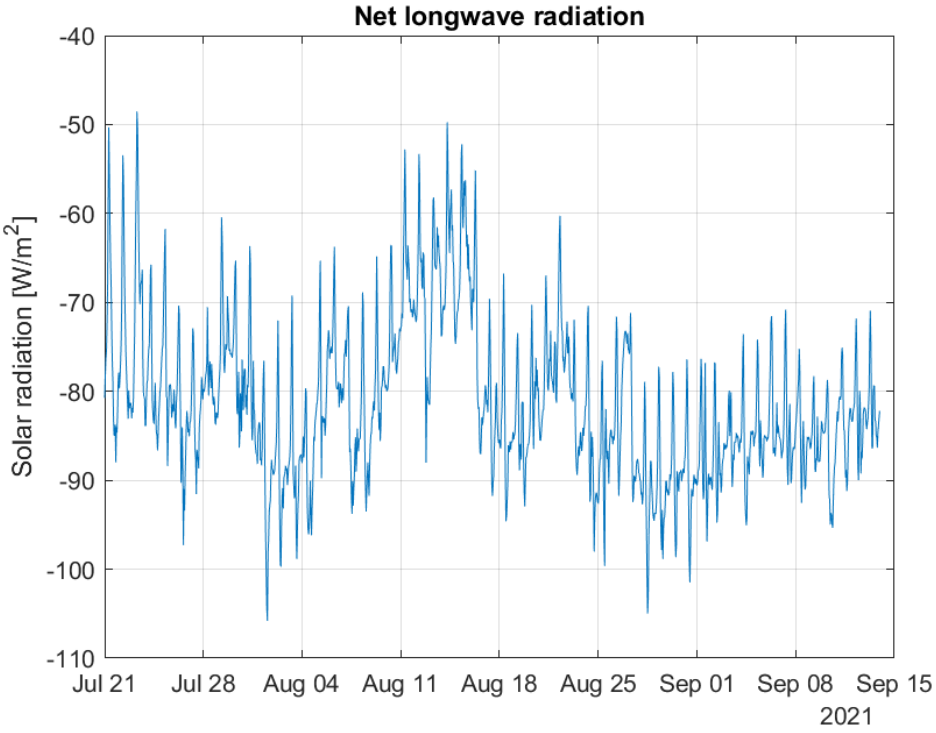

Figure 8.3: *Net longwave radiative flux.*

8.3.3 Latent heat flux

Latent heat flux depends on air temperature and on wind velocity mainly, being related to the evaporation process. Given the many bulk equations discussed in section 6.3, for

sake of simplicity and for lack of data the basic equation has been used, with some further assumptions. The main point of the use of this bulk equation is the estimation of the air humidity. The latent heat flux has a strong dependency on temperature through the saturation vapor pressure. Over water surfaces it can be assumed that the mixing ratio of water vapor at the surface is equal to the saturation mixing ratio $q*$ at the temperature of the surface

$$q_s = q*(T_s) \tag{8.4}$$

The actual vapor mixing ratio of saturated air at the reference height can be approximated with a first-order Taylor series as

$$q_a* = q*(T_s) + \frac{\partial q*}{\partial T}(T_a - T_s) + ... \tag{8.5}$$

The relative humidity at that level can be expressed in terms of actual vapor-mixing ratio of the air at the reference height

$$RH = \frac{q}{q*} \qquad q_a = RH\left(q*(T_s) + \frac{\partial q*}{\partial T}(T_a - T_s)\right) \tag{8.6}$$

Substituting Eq. 8.6 into the equation for the estimation of the latent heat flux and truncating the Taylor series at the first term, it is obtained

$$H_e = \rho_a L_e c_L V q_s (1 - RH) \tag{8.7}$$

The density of air is $\rho_a = 1.29\,\text{kg/m}^3$. To be very precise, since this water comes from a melting glacier its density should be slightly different and it should be calculated from the Snow Water Equivalent (SWE). All these data are not available, and also it is not known which is the fraction of water from the melting process that runs off the towards lakes and valley streams and the fraction that infiltrates. Latent heat of evaporation $L_e = 2260\text{KJ/Kg}$ is assumed to be reasonable. c_L is a bulk coefficient given as $c_L = 5 \times 10^{-5}$ [22]. The wind velocity V is not available at the target, since no anemometers or similar instruments are present at that location. The wind velocity time series used in the calculations is the one recorded at La Thuile - La Grand Tete station. The same reasoning holds for the relative humidity: RH time series of values recorded at La Thuile - La Grand Tete station is used. q_s is the saturation humidity ratio of air at 5° C (range of the mean lake temperature in the measured period), $q_s = 0.005$ is assumed to be a reasonable value [23].
The time series obtained for the latent heat, once plugged into the equation the above cited quantities, is showed in Figure 8.4. From the graph in Figure 8.4, it can be observed the presence of the night day cycle, even if attenuated with respect to the shortwave radiation

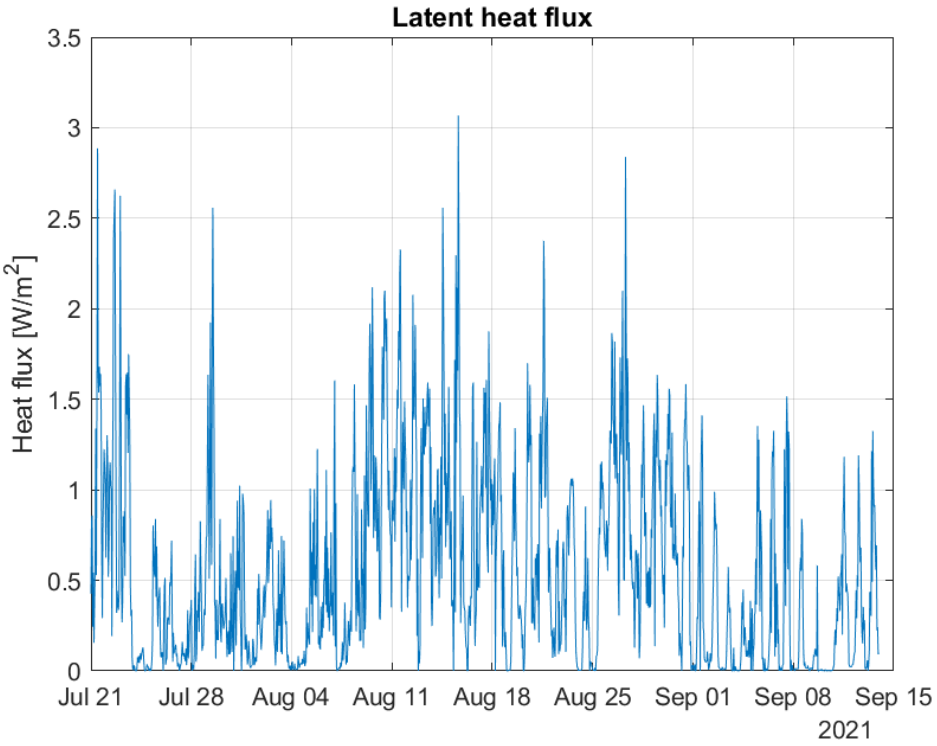

Figure 8.4: *Latent heat flux.*

plot, and a curve shape that follows slightly the shape of the longwave radiation. The link between the shape of the curve of the longwave radiation and the curve of the latent heat is due to the dependence, direct or indirect, on the water temperature.

Since latent heat flux is subtracted from the lake thermal flux, it appears with a negative term in the complete heat flux equation.

8.3.4 Sensible heat flux

Sensible heat flux is expected to be the term with the lowest contribution in magnitude to the total heat flux. The time series of the sensible heat flux has been calculated from

$$H_c = \rho_a c_p c_h V \left(T_w - T_a\right) \tag{8.8}$$

The density of air is $\rho_w = 1.29\,\mathrm{kg/m^3}$. Same assumptions as for latent have been done. c_h is a constant evaluated to be $c_h = 1 \times 10^{-3}$; c_p is the specific heat of air at constant pressure. The wind velocity series that has been used, as for latent heat flux, is the one recorded at La Thuile - La Grand Tete station.

With all the data, the time series of sensible heat flux has been estimated, and the graph in Figure 8.5 is showing the obtained result. As it can be observed from Figure 8.5, some

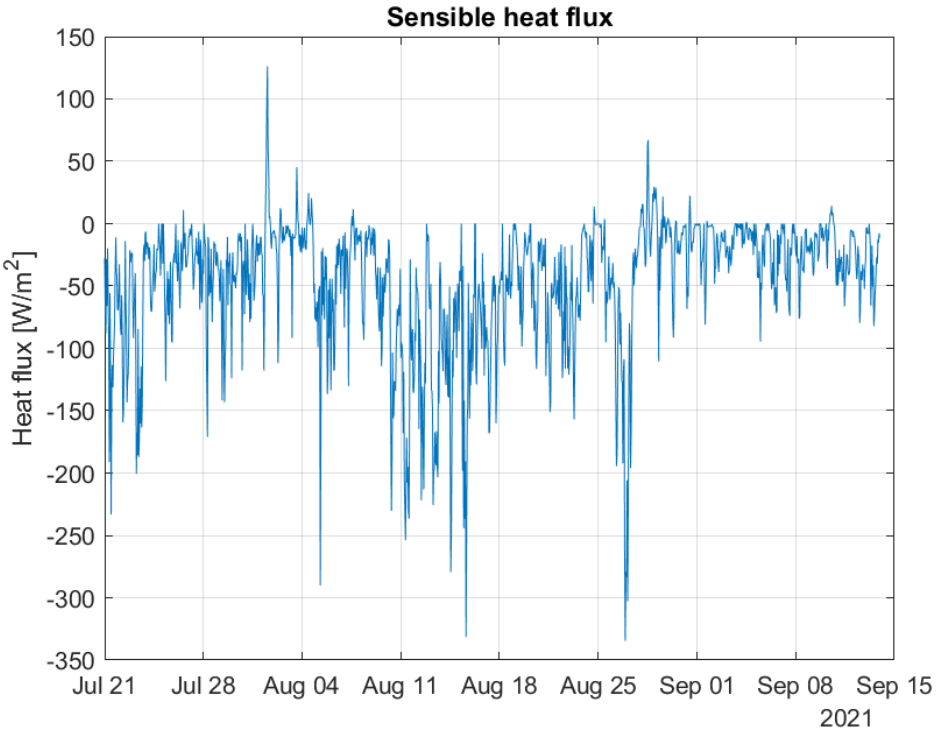

Figure 8.5: *Sensible heat flux.*

peak values are presence in correspondence to rainy days. This can be due to the very high air humidity, thus very similar values of water and air vapor pressures.

Sensible heat is a negative contribution to the thermal flux of the lake if the difference between water and air temperature is considered. In terms of reasoning, if water is warmer with respect to air the heat lost by the lake is higher, and vice versa. That's why this term appears with a negative sign within the complete heat equation.

8.3.5 Total heat flux

Once all the components have been evaluated, the total heat flux can be computed. The rived bed heat exchange component and the precipitation and tributaries effects are neglected, since they are not considered fundamental in the computations; their magnitude would not be comparable with the other factors of the total heat flux. The total heat flux is calculated as

$$H_{total} = H_{sw} + H_{lw} + H_l + H_s \tag{8.9}$$

Unfortunately the anomalous peaks appearing in the sensible heat flux time series affect the whole result. The total heat flux affecting lake water surface in time is shown in Figure 8.6. Since these anomalous peaks are present in the graph, it is not possible to well comment the total heat series.

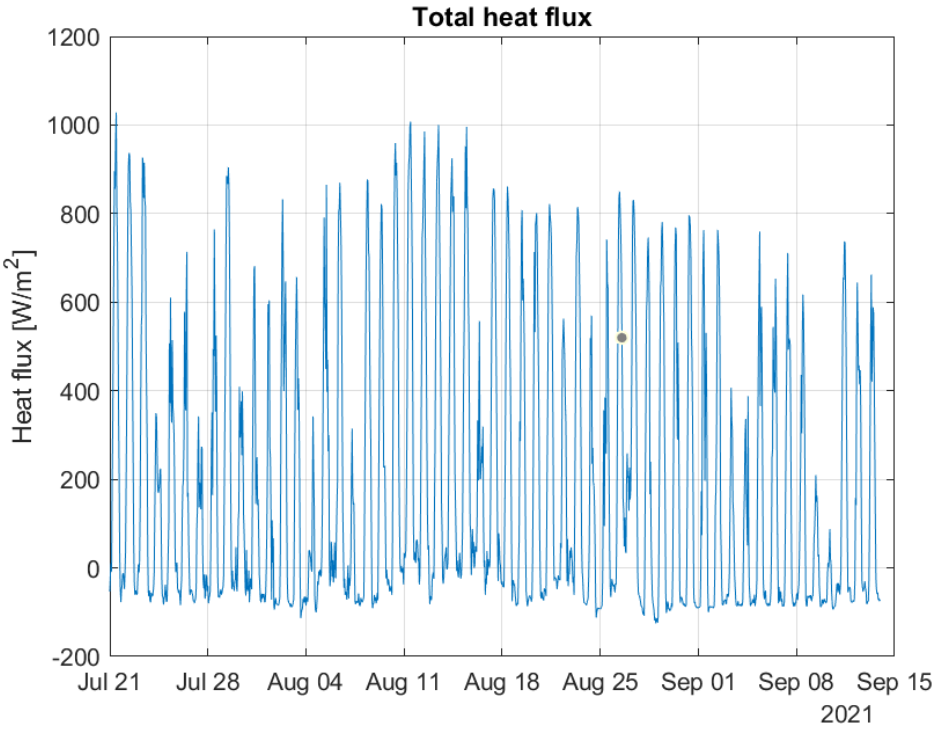

Figure 8.6: *Total heat flux*.

8.4 Complete model discussion

Once calculated the total heat exchanged and relying on the assumptions done above about the convective and the diffusive terms, the total model can be constructed integrating Eq. 8.1. The solution, given the dependency of some of the heat flux term on the water temperature is

$$T_w(t) = \frac{1}{\rho c_p} \int_0^\tau \frac{H_{total}(t)}{d} dt \tag{8.10}$$

Eq. 8.10 has been obtained from the integration over the whole lake surface of Eq. 8.1. When integrating on the whole lake surface, the numerator of the integral has to be multiplied by the lake surface, and at the denominator the lake volume mus appear. In an ideal case in which the mean lake depth is the one measured by the probe, the area can be simplified and the heat flux is only to be divided by the lake depth. d is the average lake depth, it varies in time since it is measured by the probe. It has to be corrected by an offset, since the probe was not measuring the level from the bottom of the lake. H_{total} is still in the integral because it is time dependent, as it represents the sum of all the heat fluxes.

Substituting all the different heat contribution within Eq. 8.10, one gets

$$\frac{\partial T_w}{\partial t} = \frac{1}{\rho c_p d}\left(R(1-\alpha) + \varepsilon_m \sigma T_a^4 a C^b - \varepsilon_w \sigma T_w^4 - \rho_a L_e c_L V q_s (1-RH) - \rho_a c_p c_h V (T_w - T_a)\right) \tag{8.11}$$

Where:
T_w Water temperature [°C]
ρ Water density [Kg/m^3]
c_p Specific heat of water [J/Kg °C]
d Channel depth [m]
R Solar shortwave radiation [W/m^2]
α Albedo [-]
ε_m Sky emissivity [-]
σ Stefan-Boltzmann constant [W/m^{2}K^4]
T_a Air temperature [K]
C Cloud cover (0-1) [-]
a Empirical coefficient [-]
b Empirical coefficient [-]
ε_w Water emissivity [-]
ρ_a Air density [Kg/m^3]
L_e Latent heat of vaporisation [MJ/Kg]
c_L Bulk coefficient [-]
V Wind velocity at 2 m [m/s]
q_s Saturation humidity ratio [-]
RH Relative air humidity [%]
c_h Bulk coefficient [-]

Eq. 8.11 represents the variation of water temperature of the lake at every hour, since the data have this time step. It is a non linear differential equation, thus it is solved via an iterative numerical method. Runge-Kutta method, fourth order has been used to solve the equation. Runge-Kutta algorithm is an explicit method to approximate solution of simultaneous nonlinear equation, used in time discretisation. First, the variant to represent the time derivative of the water temperature is given as

$$\frac{\partial T_w}{\partial t} = f(t, T_w) \tag{8.12}$$

The solution at the $n+1$th step is

$$T_w^{\tau+1} = T_w^{\tau} + \frac{1}{6}(k_1 + 2k_2 + 2k_3 + k_4) \tag{8.13}$$

The k_n terms in Eq. 8.13 are defined throughout the iterations as

$$k_1 = \Delta t f(t^{\tau}, T^{\tau}) \tag{8.14}$$

$$k_2 = \Delta t f\left(t^{\tau+\frac{1}{2}}, T^{\tau} + \frac{k_1}{2}\right) \tag{8.15}$$

$$k_3 = \Delta t f\left(t^{\tau+\frac{1}{2}}, T^{\tau} + \frac{k_2}{2}\right) \tag{8.16}$$

$$k_4 = \Delta t f\left(t^{\tau+1}, T^{\tau} + k_3\right) \tag{8.17}$$

The time step has to be chosen before iterations start. In this case, given that the data were provided with an hourly step, a time step (Δt) of one hour has been chosen. Runge-Kutta method at the fourth order has a local truncation error of $\mathcal{O}[(\Delta t)^5]$.

An initial condition has to be given to the numerical algorithm to start the integration in time. The first measured value has been given to the algorithm as initial condition. In Figure 8.7 the estimated series with the cited method is plotted together with the series measured with the instrument.

It is well observable that the two series have a number of differences. At a first glance it can be stated that:

- The series has the same order of magnitude of the measured values, even though the mean temperature of the estimated series is higher with respect to the real one.
- Even if some kind of night day cycle is visible, it is not as regular as in the measured series, there should be some terms in the equation that operate against the cyclicity.
- some abrupt peaks are present in the estimated series: in these moments probably one or more terms overcome the action of the others and let the series behave in this anomalous way.

To better quantify the influence of each term on the total heat flux, their values have been calculated by using the mean values of the meteorological variables. To get a general view of the order of magnitude of each term, the mean value of the measured series of water temperature has been used as mean value of T_w. The obtained results are shown in Table

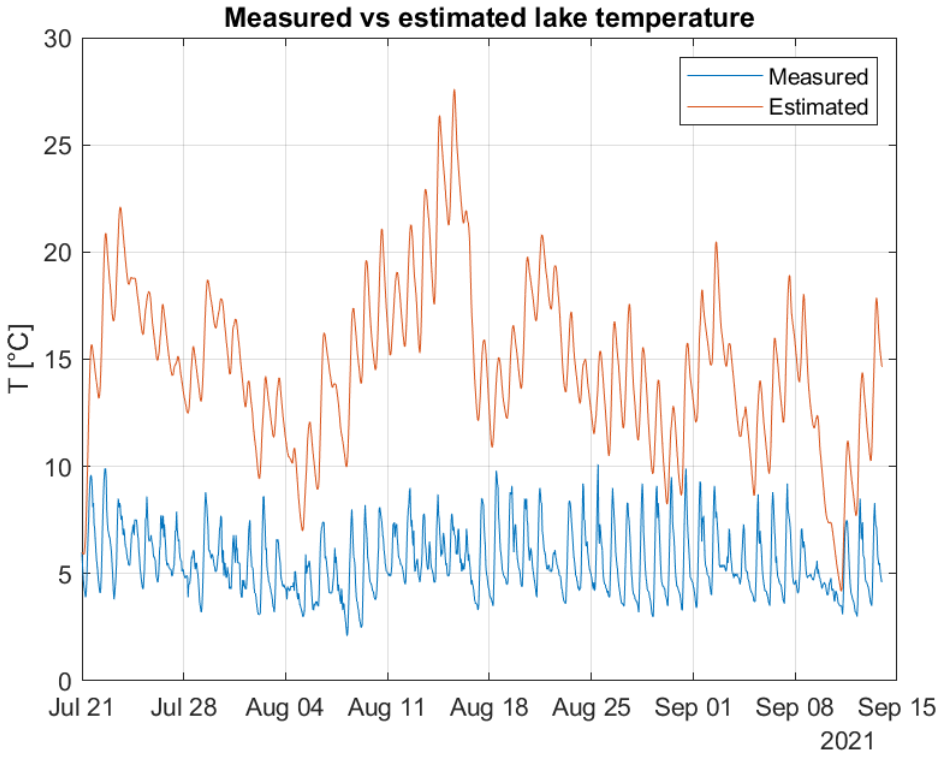

Figure 8.7: *Numerical solution found via Runge-Kutta method, vs the measured series.*

Term of the heat flux	**Expression**	**Mean value [W/m^2]**
Net shortwave radiation	$R(1-\alpha)$	220.15
Incoming longwave radiation	$\varepsilon_m C^b \sigma T_a^4$	257.3137
Outgoing longwave radiation	$-\varepsilon_w \sigma T_w^4$	-338.8005
Latent heat	$-\rho_a L_e c_L V q_s (1-RH)$	-0.5265
Sensible heat	$-\rho_a c_p c_h V (T_w - T_a)$	46.8914

Table 8.1: *Mean values of the terms of the heat flux equation.*

8.1. At a first glance it is clear as the three first terms (shortwave radiative flux and longwave incoming and outgoing radiative flux) are the one governing the equation. In an ideal behaviour assumption, the total thermal flux should compensate the entering and the exiting thermal flux from the surface, but actually it is not so. If all the terms of the table are added up, a mean positive flux of 185 W/m^2 is obtained (Figure 8.6): it means that the water is warmed up when passing through the lake, there must be a difference between the inlet water water temperature and the measured water temperature (assumed homogeneous in the lake, thus the outlet water temperature). During the same period as in 2021, in year 2022 measurements of the lake water temperature have been repeated. Temperature near the lake inlet has been measured. The mean temperature that has been recorded at the lake inlet during the measuring period is around 2.5°C. A rough measure of the lake surface can be

estimated from orthophotos, even though it mus be considered that the lake surface area is not constant during the whole measuring period. An estimation of the surface of the lake during its maximum extension, thus during summer months, can be of 6000 m^2. The mean lake depth can be assumed to be 1 m. One obtains a total water volume of 6000 m^3. At the inlet of the lake a discharge that varies between 0.5 and 4 m^3/s along the season has been measured. As an hypothesis it can be assumed a mean discharge of 1 m^3/s at the lake inlet. The temperature variation of water between the inlet and the outlet of the lake is about 3° C. To obtain an estimation of the calories needed per liter of water to warm up the entire water volume that is flowing, the entering flux has to be multiplied by the ΔT and expressed in calories. Assuming $c_p = 4.187$kJ/Kg K, the total energy needed for the whole lake to reach the mean measured temperature near the outlet is 12561 kJ. Dividing by the total volume of the lake it means that 2.09 J per liter, thus 20.9 kJ/m^3 of water are needed to balance the entering cold flux. This estimation is very rough, not completely significant since many more complex factors such as topography, water depth, lake bathymetry, water infiltration, bed heat flux and friction, should be considered for a more complete analysis.

To better understand which is the role of each term of the thermal flux in impacting on the behaviour of the estimated series, the integration has been iterated in different manners.

1. All the variables used in the integration has been kept constant (the mean value of the variables has been inserted within the equation) apart from the lake level. The integration has been performed in time and the result is shown in Figure 8.8. With respect to the series plotted in Figure 8.7 it can be noticed that some peaks are attenuated with respect to the series in which all the variables were taken into account.

2. Now the water level is kept constant (as its mean value) and the radiation only (short wave radiation) is letting variate as the measured one. What is got with the integration is plotted in Figure 8.9, together with the measured series. Observing the obtained result, it is well visible as the night day cycle is much more similar to the measured one, not many abrupt peaks are present any more. In addition, the amplitude of the series is similar to the amplitude of the measured series. What still remains as a big difference is the mean value. In general, the series assumes lower values, never reaching 30°C. What can be stated is that the short wave radiation is the one that rules the night day cycle, as expected. There must be a term that overcomes it frequently so that strange peaks appear.

3. Still keeping the water level constant, the air temperature is letting vary. What happens when integrating is plotted in Figure 8.10. What is noticed is that the night day cycle is not clear any more but the anomalous peaks appear. The air temperature value

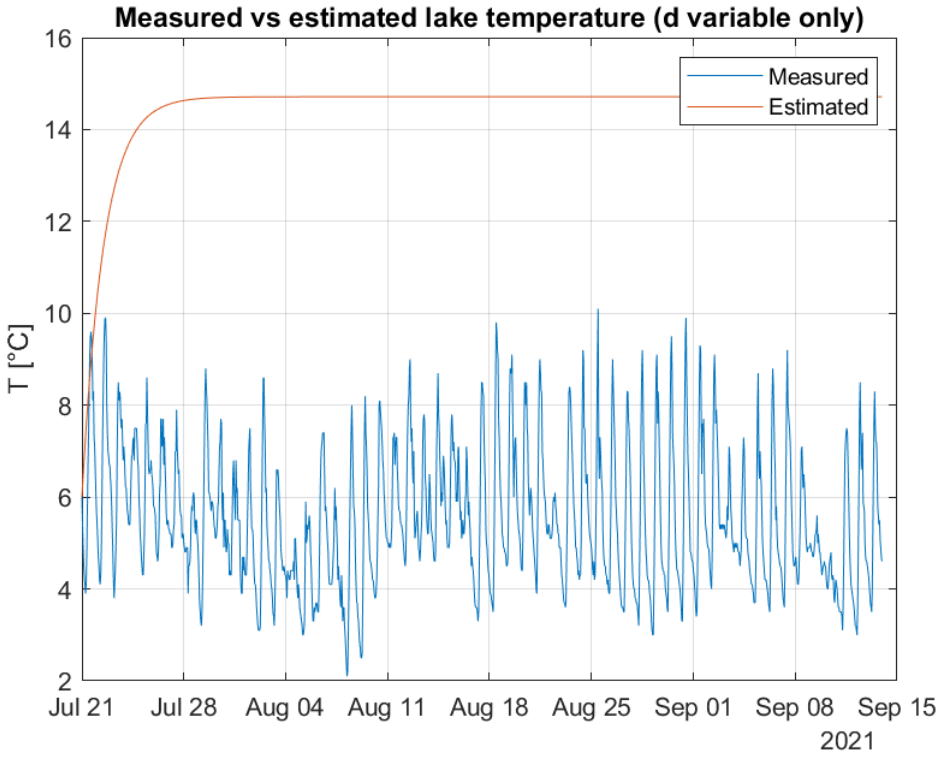

Figure 8.8: *Estimated series with only lake level as variable vs the measured series. All the others variables are kept constant as their mean value.*

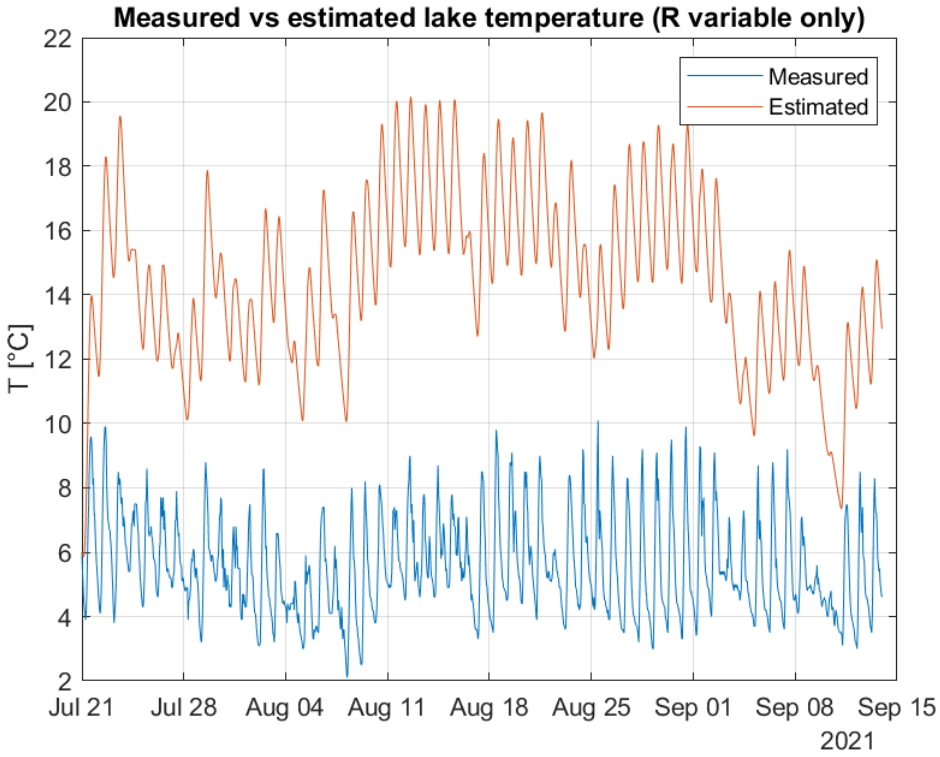

Figure 8.9: *Estimated series with only short wave incoming radiation as variable vs the measured series. All the others variables are kept constant as their mean value.*

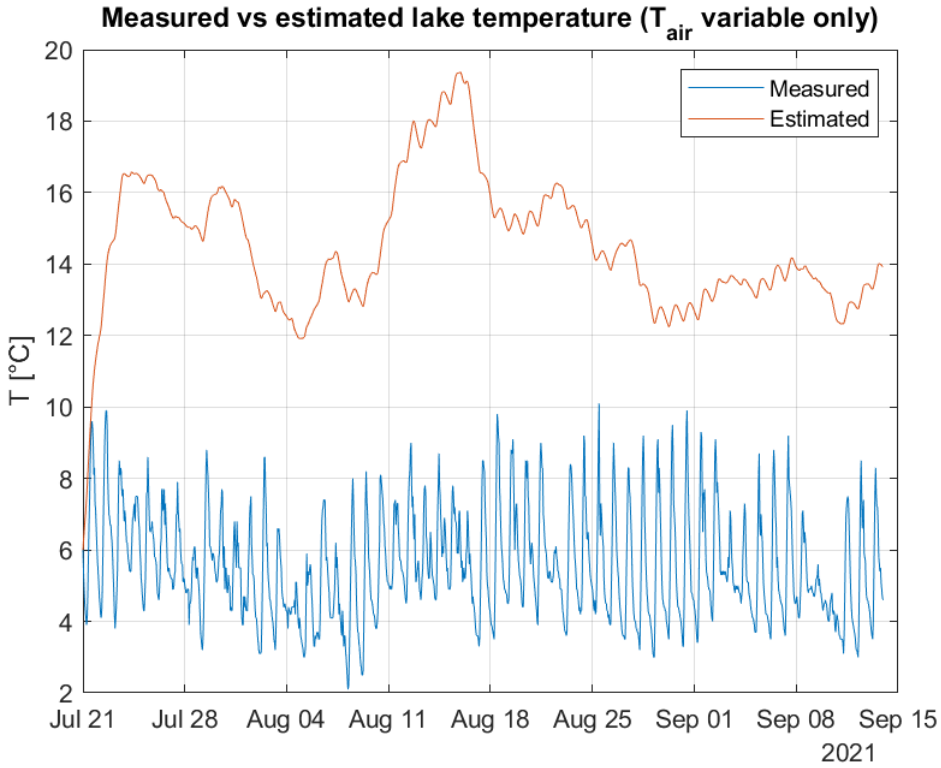

Figure 8.10: *Estimated series with only air temperature as variable vs the measured series. All the others variables are kept constant as their mean value.*

appears both in the calculation of the longwave downward flux and of the sensible heat flux. When keeping constant the air temperature in the sensible heat flux term, what is obtained by integrating is shown in Figure 8.11. Looking at Figure 8.11, it can be observed that the temperatures values are stable, oscillating around 25°C, without any weird peak. The peaks appear instead when the air temperature is kept constant for the longwave radiation term (entering the lake) but not for the sensible heat term (Figure 8.12). The behaviour can be due to the fact that the sensible heat term accounts for the difference between air and water temperature, that can be in some cases very small.

4. At last the contribution of the latent heat term is evaluated. Apparently, it can be crucial, since this is the term that is the smaller in magnitude by at least one order of magnitude with respect to the others. By keeping all the variables constant, except from the wind speed and the relative humidity in the latent heat term, what one gets as result is shown in Figure 8.13. As it can be observed, the series reaches the convergence around a certain value, and then it remains almost constant (a part from minimal fluctuations not visible from the graph). Such an evaporative flux means in terms of water evaporated from the lake a mean over the series of 8.37×10^{-4} mm. The evaporated water has been calculated by dividing the energy (latent heat flux) by

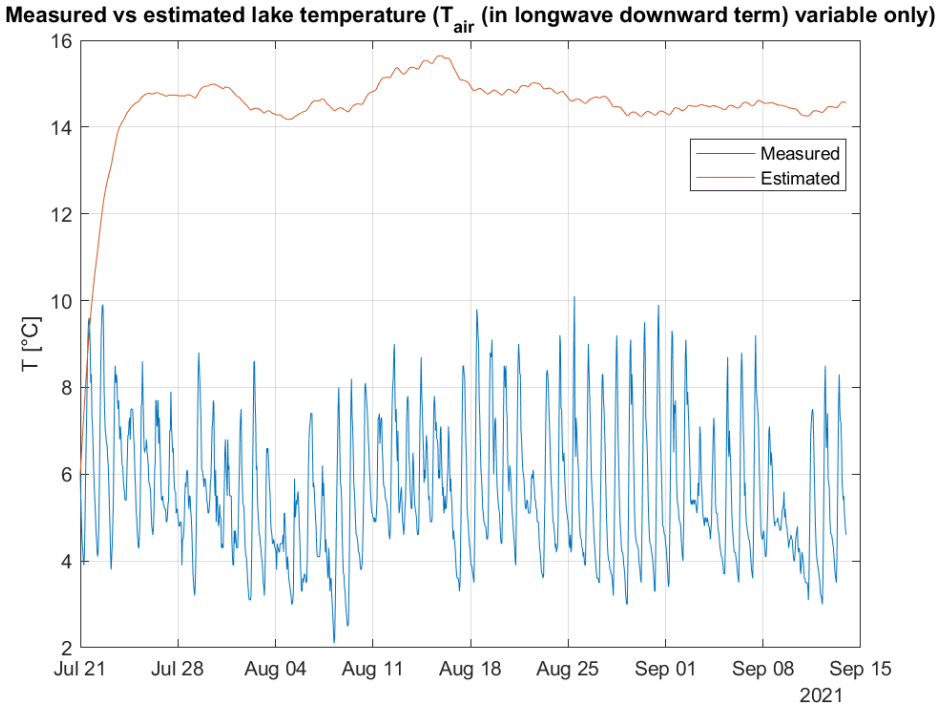

Figure 8.11: *Estimated series with only air temperature as variable (in the longwave downward term) vs the measured series. All the others variables are kept constant as their mean value.*

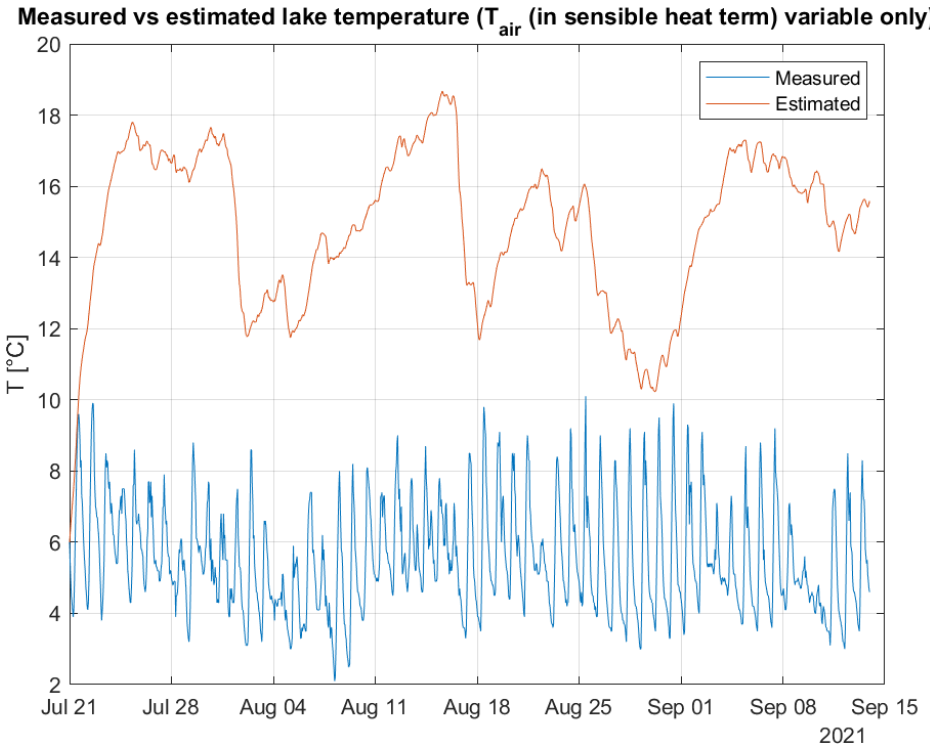

Figure 8.12: *Estimated series with only air temperature as variable (in the sensible heat term) vs the measured series. All the others variables are kept constant as their mean value.*

the latent heat of evaporation of water. This value can be realistic considering the location of the lake we are analysing data of.

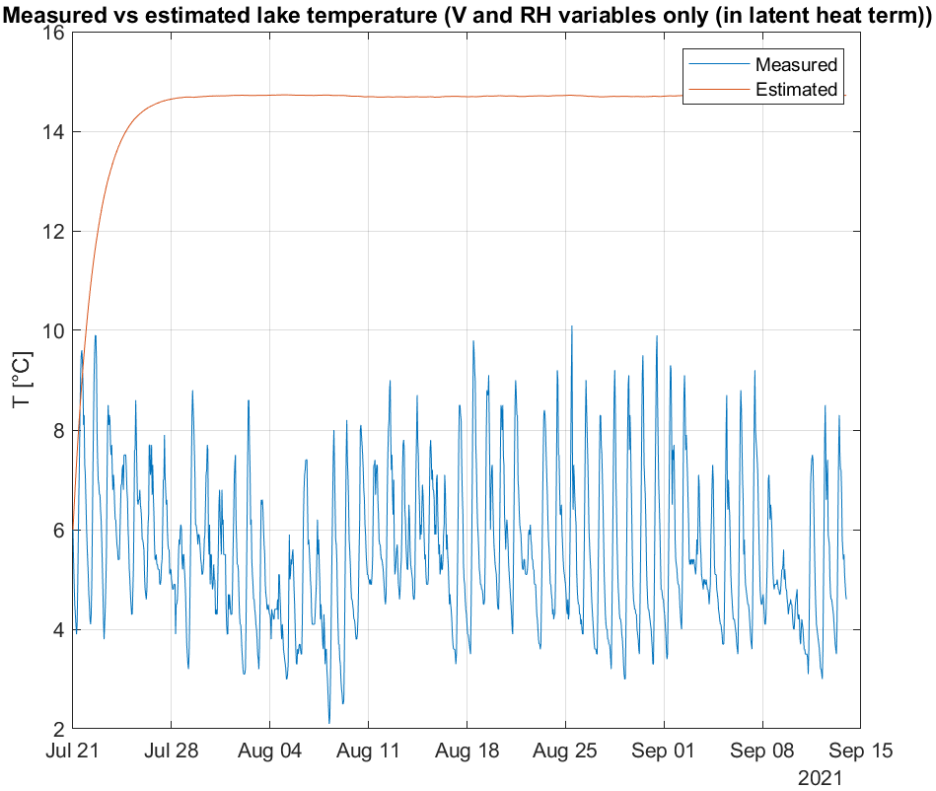

Figure 8.13: *Estimated series with only wind speed and relative humidity as variable (in the latent heat term) vs the measured series. All the others variables are kept constant as their mean value.*

After all these evaluation, it can be said that probably the sensible heat term is the one that is driving at most the anomalous behaviour of the series.

To check the robustness of the model the numerical integration has been performed by giving as initial conditions the whole series of temperatures that has been measured at the lake site. Of course, given every initial condition, only the remaining values of the series after such initial conditions were estimated, in order to have some real values to compare to. Going on through the time series the number of estimated temperatures decreases. In Figure 8.14 the first four series (giving as initial condition the first four measurements) are represented. It can be observed that the general behaviour towards convergence is similar, regardless of the initial condition. In Figure 8.15 the zoom of some points in which the different lines are visible is reported. The zoomed figure refers to the starting part of the series, in which the influence of the initial condition is stronger.

The bias present in the estimated series can be due not only to meteorological variables,

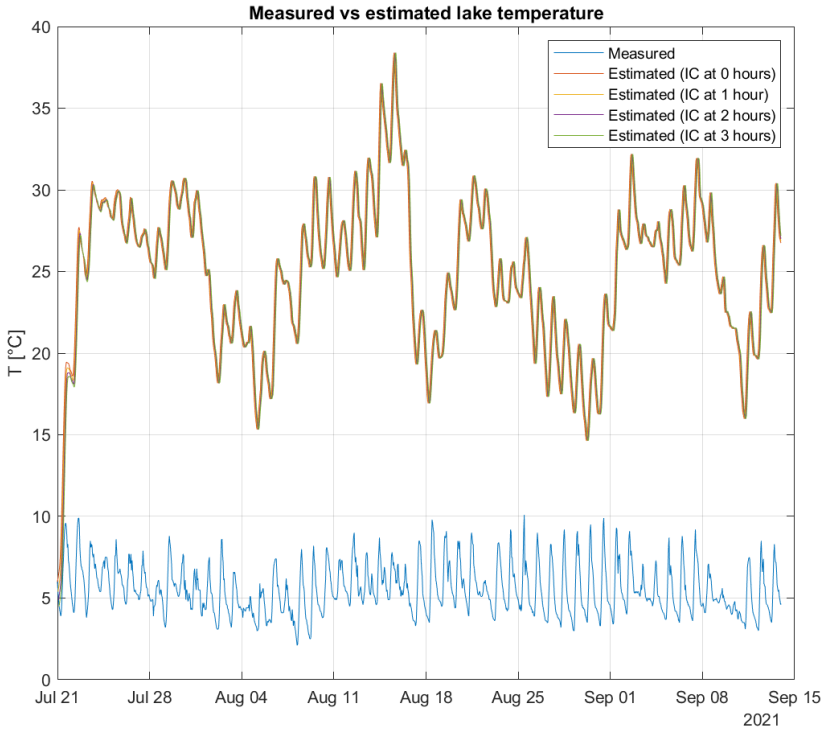

Figure 8.14: *Estimated series vs the measured one, the different series are estimated giving a different initial condition, starting from the first measured value on.*

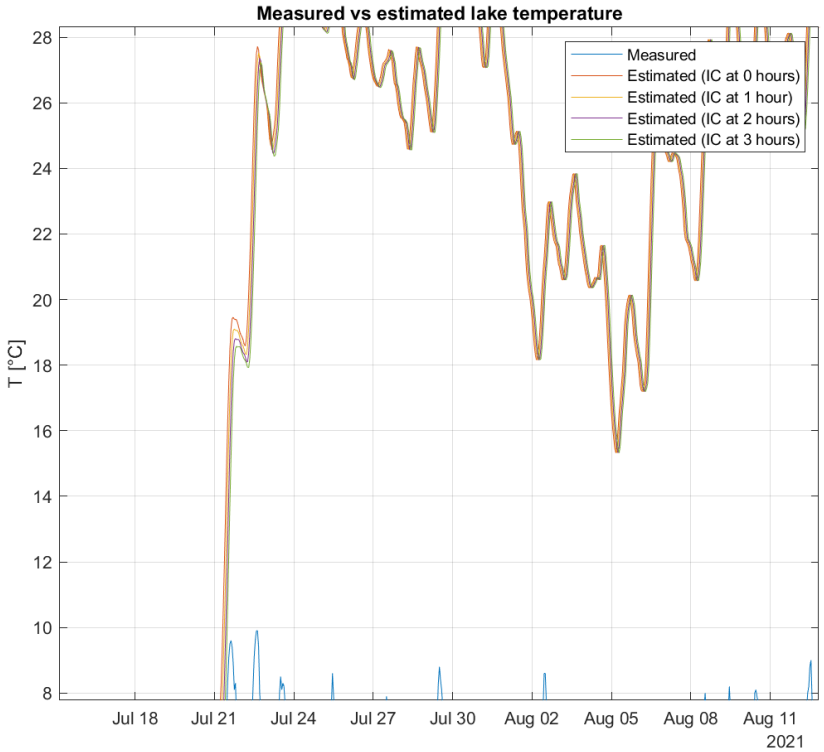

Figure 8.15: *Estimated series vs the measured one, the different series are estimated giving a different initial condition, starting from the first measured value on (zoom on the first part).*

but also to the previously defined constant terms. In Eq. 8.11, terms can be grouped into two main parts: terms depending from T_w and terms in which T_w^4 appears. Thus, Eq. 8.11 can be seen as a relaxation of Eq. 8.18.

$$\frac{\partial T_w}{\partial t} = C_1 T_w^4 + C_2 T_w \tag{8.18}$$

where:

$$C_1 = \varepsilon_w \sigma \qquad C_2 = \rho_a c_p c_h V \tag{8.19}$$

keeping V (wind velocity) constant as its mean value. C_1 and C_2 are evaluated (keeping V constant) as

$$C_1 = 5.6137 \times 10^{-8} W/m^2K^4 \qquad C_2 = 15.1481 W/m^2K \tag{8.20}$$

Looking at the obtained values, it is clear that the weight of the term at the fourth power is less relevant with respect to the sensible heat term. As from Table 8.1, the other terms that are contributing in a substantial way to the total flux equation are the shortwave net flux and the longwave incoming and outgoing flux.

At first, sensibility of α (albedo) has been checked by both increasing and decreasing the parameter in the equation. Not sensible changes in the mean value of the estimated series (to avoid the bias) is observed (Figure 8.16). As second trial the constant in front of the fourth

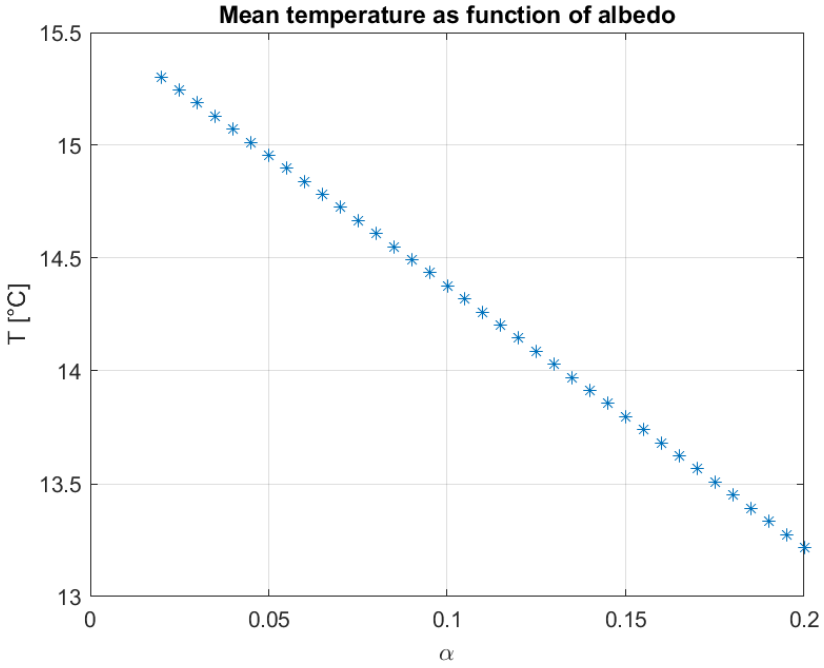

Figure 8.16: *Mean temperature value as α is varying from the original value ($\alpha = 0.07$).*

power of the air temperature has been tuned. The weakest part of this term is the cloud cover

factor. By changing the exponent b, very little change sin the total value are observed, since C^b is very close to 1. To reduce the total longwave downward term the b exponent should be turned into a positive one. By keeping $b = -0.0227$, the cloud cover factor results in 1.0277. If the multiplication is performed, it means that on average clouds contribute with a +7.1276 W/m^2. The resulting cloud forcing is compliant with other measurements in the Alpine region found in literature [31] [27]. It can be observed that a mean of cloud cover has been used: for a sky completely covered by clouds, the cloud forcing would be higher. In order to remove the bias of the mean of the estimated series, with respect to the measured one, a constant term in the total heal flux, such as to balance the heat exchange has been inserted. A mean flux of 185 W/m^2 has been removed from the total heat flux, so that the summation of all the mean terms contributing to the heat flux sums up to zero. The resulting series is plotted in Figure 8.17. Such term, that has been removed from the total heat flux to

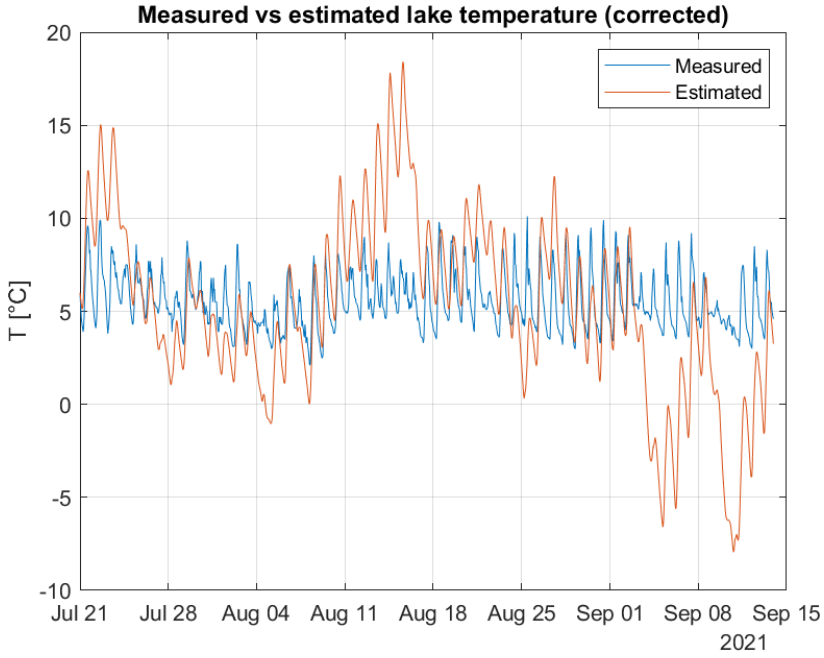

Figure 8.17: *Estimated temperature series vs the measured one, with mean correction.*

balance the energy, in principle can be due to the cold water entering the lake. If calculations made before of the energy needed to warm up the entering cold water are in the right order of magnitude, some other contribution must be considered, to get a final balance of that order of magnitude. The bed friction and the groundwater heat exchange, as well as the rainfall water contribution can't in principle be neglected.

Looking at all the series of data available for the analysis, what can be noticed (cfr. Figure 7.7) is that in correspondence of raining events the estimated temperature is lower with respect to the measured one. This fact can be due to the air humidity factor appearing in the latent heat term, that must be recalled it is not the air humidity at the lake location but

at a near site with comparable height.
At the beginning of the series and at mid August, the temperatures estimated were higher with respect to the measured ones. It seems that no significant precipitation events were recorded in the area. What can be observed though (Figure 7.6) is that in these two periods the air temperatures were the highest in the whole series at all the considered stations. Since the air temperature is appearing within the model equation in one of the driving terms, the peaks observed in Figure 8.7 at the beginning of the series and at mid August can be due to this remarkable contribution.

Since the high peaks appears in days in which the air temperature is very high, and probably the thermal flux at the surface is intense, it may be that considering the thermal flux entering and exiting the target lake is crucial to estimate in a good way the water temperature. In days in which the air temperature is high the melting process is in general accelerated. The amount of water that is both infiltrating below the surface and running off towards the lake is greater, thus an estimation of the thermal flux due to water flux in and out the lake can probably explain the introduction of these peaks. This hypothesis is partially confirmed by looking at the water level series (Figure 7.4). The water level is high when rainfall occurs but also when air temperature is high, even if this second correspondence is not as visible as the first one. A measure of the water velocity at the inlet and the outlet of the lake can be useful to validate such an hypothesis. Furthermore, it has to be considered that the work is analysing a seasonal lake, thus the areal dimension is changing due to the amount of water running off from the glacier tongue. The water level is for sure influenced by the area of the lake.
Another contribution that has been neglected but that should have been taken into account is the lake bed and banks contribution: infiltration of water below the surface should be quantified, as well as the structure of the soil below the lake bottom, and of the periglacial area. To estimate how much water infiltrates, it can be useful the estimation of snow water equivalent and the calculation of the volume of water in the lake, with a time step short enough to detect the lake shrinkage or enlargement due to the different melting rate.

9. Conclusion

The obtained series has still some differences with respect to the measured one. Apart from the latent heat term that is the cause of the input of some anomalous peaks, the series copies quite well the night/day cycle of the measured series. This behaviour means that in some way the delay of the water temperature with respect to air temperature detected with the statistical analysis of the data has been respected. Considering adiabatic banks and bed of the lake and neglecting the contributions to the heat flux of rainfall and incoming water at the inlet, for sure has influenced the solution. Water flowing within the lake and underground, coming from the glacier melting is probably very cold. Regardless to air temperature, the amount water running from the bottom part of the glacier, its velocity and temperature, should in some be quantified to get a more detailed solution of the created model.

Bibliography

[1] URL: https://www.arpa.vda.it/it/relazione-stato-ambiente/archivio-rsa/xiv-relazione-sullo-stato-dell-ambiente-2019/1322-rsa-2019-ambiente-naturale/rsa-2019-criosfera-e-biosfera/3575-bilancio-di-massa-dei-ghiacciai-ambceb002.

[2] URL: https://www.arpa.vda.it/en/archivio-news/3817-la-scarsit%C3%A0-di-precipitazioni-invernali-confermata-dalle-misure-di-accumulo-nevoso-sui-ghiacciai.

[3] URL: http://www.nimbus.it/glaciorisk/Glacier_view.asp?IdGlacier=1455&Vista=paese&Paese=italy&IdTipoRischio=.

[4] URL: https://presidi2.regione.vda.it/str_dataview.

[5] X Berger and J Bathiebo. "Directional spectral emissivities of clear skies". In: *Renewable Energy* 28.12 (2003), pp. 1925–1933. ISSN: 0960-1481. DOI: https://doi.org/10.1016/S0960-1481(03)00059-4.

[6] Piero Boccardo. "Remote Sensing basics - Spectral signatures". In: (2021), pp. 75–78.

[7] I.S. Bowen. "The ratio of heat losses by conduction and by evaporation from any water surface". In: *Physical Review* 27.6 (1926), pp. 779–787. DOI: 10.1103/PhysRev.27.779.

[8] George Box. "Box and Jenkins: Time Series Analysis, Forecasting and Control". In: Jan. 2013, pp. 161–215. ISBN: 978-1-349-35027-8. DOI: 10.1057/9781137291264_6.

[9] H. A. R. de Bruin. "A Simple Model for Shallow Lake Evaporation". In: *Journal of Applied Meteorology (1962-1982)* 17.8 (1978), pp. 1132–1134. ISSN: 00218952, 2163534X.

[10] H. A. R. de Bruin and J. Q. Keijman. "The Priestley-Taylor Evaporation Model Applied to a Large, Shallow Lake in the Netherlands". In: *Journal of Applied Meteorology (1962-1982)* 18.7 (1979), pp. 898–903. ISSN: 00218952, 2163534X.

[11] Wilfried Brutsaert. “On a derivable formula for long-wave radiation from clear skies”. In: *Water Resources Research* 11.5 (1975), pp. 742–744. DOI: https://doi.org/10.1029/WR011i005p00742.

[12] Wilfried Brutsaert and Han Stricker. “An advection-aridity approach to estimate actual regional evapotranspiration.” In: *Water Resources Research* 15 (1979), pp. 443–450.

[13] D. CAISSIE. “The thermal regime of rivers: a review”. In: *Freshwater Biology* 51.8 (2006), pp. 1389–1406. DOI: https://doi.org/10.1111/j.1365-2427.2006.01597.x.

[14] Jonathan L. Carrivick et al. “Toward Numerical Modeling of Interactions Between Ice-Marginal Proglacial Lakes and Glaciers”. In: *FRONTIERS IN EARTH SCIENCE* 8 (Oct. 2020). DOI: 10.3389/feart.2020.577068.

[15] J. Graham Cogley. “The Albedo of Water as a Function of Latitude”. In: *Monthly Weather Review* 107.6 (1979), pp. 775–781. DOI: 10.1175/1520-0493(1979)107<0775:TAOWAA>2.0.CO;2.

[16] Grace J. Di Cecco and Tarik C. Gouhier. “Increased spatial and temporal autocorrelation of temperature under climate change”. In: *SCIENTIFIC REPORTS* 8 (Oct. 2018). ISSN: 2045-2322. DOI: 10.1038/s41598-018-33217-0.

[17] Stephen J. Dugdale, David M. Hannah, and Iain A. Malcolm. “River temperature modelling: A review of process-based approaches and future directions”. In: *EARTH-SCIENCE REVIEWS* 175 (Dec. 2017), pp. 97–113. ISSN: 0012-8252. DOI: 10.1016/j.earscirev.2017.10.009.

[18] Dominique Dumas. “Changes in temperature and temperature gradients in the French Northern Alps during the last century”. In: *Theoretical and Applied Climatology* 111 (Jan. 2013), pp. 223–233. DOI: 10.1007/s00704-012-0659-1.

[19] EC Evans, GR McGregor, and GE Petts. “River energy budgets with special reference to river bed processes”. In: *HYDROLOGICAL PROCESSES* 12.4 (Mar. 1998), pp. 575–595. ISSN: 0885-6087.

[20] Blandine Georges et al. “Which environmental factors control extreme thermal events in rivers? A multi-scale approach (Wallonia, Belgium)”. In: *PEERJ* 9 (Nov. 2021). ISSN: 2167-8359. DOI: 10.7717/peerj.12494.

[21] Guy Earl Harbeck, Max A. Kohler, and Gordon E. Koberg. “Water-loss investigations; Lake Mead studies”. In: 1958.

[22] Jost von Hardenberg. “The climate system - Radiative forcing and energy balance in the climate system”. In: (2021), pp. 30–35.

[23] Dennis L. Hartmann. “Chapter 1 - Introduction to the Climate System”. In: *Global Physical Climatology (Second Edition)*. Ed. by Dennis L. Hartmann. Second Edition. Boston: Elsevier, 2016, pp. 1–23. ISBN: 978-0-12-328531-7. DOI: https://doi.org/10.1016/B978-0-12-328531-7.00001-3.

[24] Ashish Karn, Venkateshwarlu Chintala, and Suresh Kumar. “An investigation into sky temperature estimation, its variation, and significance in heat transfer calculations of solar cookers”. In: *Heat Transfer—Asian Research* 48.5 (2019), pp. 1830–1856. DOI: https://doi.org/10.1002/htj.21459.

[25] Christa Kelleher, Heather Golden, and Stacey Archfield. “Monthly river temperature trends across the US confound annual changes”. In: *Environmental Research Letters* 16 (Oct. 2021), p. 104006. DOI: 10.1088/1748-9326/ac2289.

[26] Mark A. Kirk and Frank J. Rahel. “Air temperatures over-predict changes to stream fish assemblages with climate warming compared with water temperatures”. In: *Ecological Applications* 32.1 (2022), e02465. DOI: https://doi.org/10.1002/eap.2465.

[27] T. Konzelmann et al. “Energy Balance and Evapotranspiration in a High Mountain Area during Summer”. In: *Journal of Applied Meteorology - J APPL METEOROL* 36 (July 1997), pp. 966–973. DOI: 10.1175/1520-0450(1997)036<0966:EBAEIA>2.0.CO;2.

[28] Benjamin H. Letcher et al. “A hierarchical model of daily stream temperature using air-water temperature synchronization, autocorrelation, and time lags”. In: *PEERJ* 4 (Feb. 2016). ISSN: 2167-8359. DOI: 10.7717/peerj.1727.

[29] Caccianiga M. et al. “Indagini sulla flora del Ghiacciaio del Rutor (La Thuile-AO)”. In: *Revue Valdôtaine d’Histoire Naturelle* 56 (2002), pp. 15–35.

[30] Woolway R.I. et al. Maberly S.C. O’Donnell R.A. “Global lake thermal regions shift under climate change”. In: *Nature Commun* 1232.11 (2020). DOI: 10.1038/s41467-020-15108-z.

[31] Christoph Marty et al. “Altitude dependence of surface radiation fluxes and cloud forcing in the alps: Results from the alpine surface radiation budget network”. In: *Theoretical and Applied Climatology* 72 (Jan. 2002), pp. 137–155. DOI: 10.1007/s007040200019.

[32] F. Navarro-Serrano et al. “Estimation of near-surface air temperature lapse rates over continental Spain and its mountain areas”. In: *International Journal of Climatology* 38.8 (2018), pp. 3233–3249. DOI: https://doi.org/10.1002/joc.5497.

[33] M. Olson and S. Rupper. “Impacts of topographic shading on direct solar radiation for valley glaciers in complex topography”. In: *The Cryosphere* 13.1 (2019), pp. 29–40. DOI: 10.5194/tc-13-29-2019. URL: https://tc.copernicus.org/articles/13/29/2019/.

[34] Matthew Olson, Summer Rupper, and David E. Shean. “Terrain Induced Biases in Clear-Sky Shortwave Radiation Due to Digital Elevation Model Resolution for Glaciers in Complex Terrain”. In: *Frontiers in Earth Science* 7 (2019). ISSN: 2296-6463. DOI: 10.3389/feart.2019.00216.

[35] Valerie Ouellet et al. “River temperature research and practice: Recent challenges and emerging opportunities for managing thermal habitat conditions in stream ecosystems”. In: *Science of The Total Environment* 736 (2020), p. 139679. ISSN: 0048-9697. DOI: https://doi.org/10.1016/j.scitotenv.2020.139679.

[36] Valerie Ouellet et al. “Water temperature modelling in a controlled environment: comparative study of heat budget equations”. In: *HYDROLOGICAL PROCESSES* 28.2 (Jan. 2014), pp. 279–292. ISSN: 0885-6087. DOI: 10.1002/hyp.9571.

[37] Michael Paul et al. “A Review of Water Quality Responses to Air Temperature and Precipitation Changes 1: Flow, Water Temperature, Saltwater Intrusion”. In: *JAWRA Journal of the American Water Resources Association* 55 (Dec. 2018). DOI: 10.1111/1752-1688.12710.

[38] Christian Rolland. “Spatial and Seasonal Variations of Air Temperature Lapse Rates in Alpine Regions”. In: *Journal of Climate* 16.7 (2003), pp. 1032–1046. DOI: 10.1175/1520-0442(2003)016<1032:SASVOA>2.0.CO;2.

[39] Thomas R. Sinclair. ““Natural Evaporation from Open Water, Bare Soil and Grass” by Harold L. Penman, Proceedings of the Royal Society of London (1948) A193:120–146”. In: *Crop Science* 59.6 (2019), pp. 2297–2299. DOI: https://doi.org/10.2135/cropsci2019.05.0292.

[40] Robert B. Stewart and Wayne R. Rouse. “A simple method for determining the evaporation from shallow lakes and ponds”. In: *Water Resources Research* 12.4 (1976), pp. 623–628. DOI: https://doi.org/10.1029/WR012i004p00623.

[41] Michiaki Sugita and Wilfried Brutsaert. “Cloud effect in the estimation of instantaneous downward longwave radiation”. In: *Water Resources Research* 29.3 (1993), pp. 599–605. DOI: https://doi.org/10.1029/92WR02352.

[42] Michelle T.H. van Vliet et al. “Global river discharge and water temperature under climate change”. In: *Global Environmental Change* 23.2 (2013), pp. 450–464. ISSN: 0959-3780. DOI: https://doi.org/10.1016/j.gloenvcha.2012.11.002.

[43] Cristina Viani et al. “Potential future lakes from continued glacier shrinkage in the Aosta Valley Region (Western Alps, Italy)”. In: *Geomorphology* 355 (2020), p. 107068. ISSN: 0169-555X. DOI: https://doi.org/10.1016/j.geomorph.2020.107068.

[44] Bruce W. Webb et al. “Recent advances in stream and river temperature research”. In: *Hydrological Processes* 22.7 (2008), pp. 902–918. DOI: https://doi.org/10.1002/hyp.6994.